10-6-2021 1:00 PM

Regional lipid expression abnormalities identified using MALDI IMS correspond to MRI-defined white matter hyperintensities within post-mortem human brain tissue.

William J. Pinsky, *The University of Western Ontario*

Supervisor: Whitehead, Shawn N., *The University of Western Ontario*
Co-Supervisor: Walton, Paul, *The University of Western Ontario*
A thesis submitted in partial fulfillment of the requirements for the Master of Science degree in Anatomy and Cell Biology

ABSTRACT

Periventricular white matter hyperintensities (pvWMHs) are a neurological feature detected with magnetic resonance imaging (MRI) and are clinically associated with an increased risk of stroke and dementia. pvWMHs are characterized by white matter lesions with myelin and axon rarefaction, and as such likely involve changes in lipid composition, however these alterations remain unknown. Lipids are critical in determining cell function and survival, although their detection within tissue, until recently has been challenging. Perturbations in lipid expression have previously been associated with neurological disorders. Matrix-assisted laser desorption/ionization (MALDI) imaging mass spectrometry (IMS) is an emerging technique for untargeted, high-throughput investigation of lipid expression and spatial distribution *in situ*, however the use of MALDI IMS has been previously been limited by the need for non-embedded, non-fixed, fresh-frozen samples. Work within this thesis demonstrates the novel use of MALDI IMS to distinguish regional lipid abnormalities that correlate with MRI defined pvWMHs within ammonium formate washed, formalin-fixed human archival samples. MALDI IMS scans were conducted in positive or negative ion detection mode on tissue sublimated with 2,5-dihydroxybenzoic acid or 1,5- diaminonaphthalene matrices, respectively. Using a broad, untargeted approach to lipid analysis we consistently detected 116 lipid ion species in 21 tissue blocks from 11 different post-mortem formalin-fixed human brains. Comparing the monoisotopic mass peaks of these lipid ions elucidated significant differences in lipid expression between pvWMHs and NAWM for 31 lipid ion species. Expanding our understanding of alterations in lipid composition will provide greater knowledge of

molecular mechanisms underpinning ischemic white matter lesions and provides the potential for novel therapeutic interventions targeting lipid composition abnormalities.

Keywords: CNS, MRI, pvWMHs, neurodegeneration, MALDI TOF IMS, lipids, lipidomics, multimodal imaging

SUMMARY FOR LAY AUDIENCE

Diseases of the brain, such as Alzheimer's disease and stroke, represent a major cause of disability and death, yet many remain uncurable. This is partly due to a limited understanding of molecular changes that underlie diseases. Of the three categories of biological macromolecules, which are proteins, lipids, and carbohydrates, lipids are the most abundant in the brain, accounting for 60% of the dried mass. These lipids contribute to numerous aspects of cells in the brain including forming the structural walls of cells and influencing the behaviour of cells. Due to the abundance of lipids in the brain and their ability to influence cells, they are particularly likely to be altered in diseases of the brain. Previous studies have demonstrated that changes in lipids are part of many diseases of the brain, but our understanding still remains limited. This limited understanding is partially due to the difficulty of studying the enormous variety of lipids that occur in the brain. Recent improvements in mass spectrometry, a technique for studying lipids, have opened a door for investigating changes in lipids within diseased brains. In this thesis, we use this technique to identify lipid abnormalities within diseased post-mortem human brains. By doing so, we aim to establish a workflow that will allow others to study changes in lipids that are associated with clinically observable diseases. Research into these lipid changes may identify therapeutic targets to help manage or cure neurological diseases.

STATEMENT OF CO-AUTHORSHIP

The following people and institutions contributed to the publication of work undertaken as part of this thesis:

Work in this thesis was published in Analytical Chemistry. W.P., A.R., A.H., and S.W. conceived and designed experiments. A.R. and A.K. conducted all MRI investigations. W.P., and A.R. performed all MALDI IMS, and MS/MS experiments. S.P. contributed post-mortem human tissue. K.J. and K.Y. provided technical MALDI expertise. W.P. analyzed data, wrote the manuscript and performed revisions. All authors read, edited, and approved the manuscript.

DEDICATION

To my grandparents and all others who have suffered dementia.

The memories you lost live on with us.

ACKNOWLEDGEMENTS

Thank you to my supervisor and mentor, Dr. Shawn Whitehead, I am grateful for the opportunity to participate in your research program at the Vulnerable Brain Lab. You've consistently supported my development and independence throughout the past few years with an excellent balance of patience and pressure. I will always appreciate the skills which I have developed during my time at VBL, thank you.

To all members of VBL, past and present, including A.R., A.H., V.J., B.R., W.W. and N.O., thank you for the wonderful collaborative environment which you all provided. Whether it was assistance with an experiment, discussion of experiment designs, or a hallway conversation, those interactions were a major support throughout my time at VBL. Special thanks to Dr. Lynn Wang, your tireless contributions to the lab are absolutely essential for all of our projects.

Thank you, Kristina Jurcic, for educating me on many aspects of MALDI IMS. Your work to keep the MALDI instrument running smoothly will always be appreciated.

To my parents, my family, and my friends, I wouldn't be here without your support. Mum and Dad, there are no words that can express my gratitude for all you've done throughout my life. Thank you for supporting and encouraging me as I've obtained my degrees, the next degree will probably be my last big one!

TABLE OF CONTENTS

Abstract ii
Summary for Lay Audience iii
Statement of Co-Authorship iv
Dedication v
Acknowledgements v
Table of Contents vi
List of Figures viii
List of Tables viii
List of Abbreviations ix
Chapter 1: Introduction 1
1.1. The Brain and Neurodegeneration 1
1.1.2 Neuroimaging 1
1.2. White Matter Hyperintensities 2
1.3 Lipids 3
1.3.1 Lipids in Cell Membranes 4
1.3.2 Functions – Structural 5
1.3.3 Functions – Signalling 8
1.3.4 The involvement of lipids in diseases of the CNS 10
1.4 Mass Spectrometry 11
1.4.1 Imaging mass spectrometry 11
1.4.2 MS Ion Sources 12
1.4.3 Ion sources - ESI 13
1.4.4 Ion sources - MALDI 14
1.4.5 Limitations of MALDI 15
1.4.6 Mass analyzers 16
1.4.7 Time-of-flight mass analyzers 17
1.4.8 Ion identification and MALDI TOF/TOF tandem mass spectrometry 17
1.4.9. MALDI IMS of lipids 20
1.4.10 Tissue preservation and MALDI IMS 21
1.5 Rationale 23

1.6 Aim and Hypothesis 23
Chapter 2: Methods 24
2.1 Specimen Selection for MRI Imaging 24
2.2 MRI Brain Imaging 24
2.3 Specimen Selection for MALDI TOF IMS Scanning 25
2.4 Tissue blocking 25
2.5 Tissue Sectioning and Mounting 25
2.6 Ammonium Formate Wash 26
2.7 Matrix Sublimation 26
2.8 MALDI-TOF-IMS 26
2.9 Image and Data Analysis 26
2.10 Identification of Lipid Ions by Searching Experimental m/z in LMISSD and SwissLipids 27
2.11 Identification of Previously Unidentified Mass Peaks by MALDI TOF Tandem Mass Spectrometry 28
2.12 Statistical Analysis 28
Chapter 3: Results 29
3.1 Lipid Detection Metrics 29
3.2 Negative ion MALDI IMS scans detect regional lipid abnormalities within pvWMHs – m/z 1000-2000 Range 31
3.3 Negative ion MALDI IMS scans detect regional lipid abnormalities within pvWMHs – *m/z* 450-1000 Range 35
3.4 Regional phosphatidylcholine and sphingomyelin abnormalities detected using positive ion MALDI IMS scans within pvWMHs 39
Chapter 4: Discussion 42
Conclusions 45
References 46
Appendix 64
Supplementary Figures 64
Permission 64
Curriculum Vitae 65

LIST OF FIGURES

Figure 1. Select examples of the biophysical influence of lipids on lipid membranes.

Figure 2. Schematic of the process of matrix deposition, desorption, and ionization in MALDI MS.

Figure 3. Schematic of mass analysis by TOF following MALDI.

Figure 4. Annotated MALDI-TOF mass spectra of post-mortem human white matter.

Figure 5. High range negative ion detection MALDI IMS scans distinguished increased and decreased lipid ion intensity in pvWMHs relative to NAWM in post-mortem human tissue.

Figure 6. Annotated MSMS characterization of GM1 36:1 (d18:0).

Figure 7. Low range negative ion detection MALDI IMS scans distinguished increased and decreased lipid ion intensity in pvWMHs relative to NAWM in post-mortem human tissue.

Figure 8. Low range positive ion detection MALDI IMS scans distinguished increased and decreased lipid ion intensity in pvWMHs relative to NAWM in post-mortem human tissue.

LIST OF TABLES

Table 1. Summary of characteristic negative ion lipid fragments.

Table 2. MALDI IMS lipid detection analytics.

Table 3. Identification of lipid ions, negative high range.

Table 4. Identification of lipid ions, negative low range.

Table 5. Identification of lipid ions, positive low range.

Supplementary Table 1. Demographic data from specimen selection.

LIST OF ABBREVIATIONS

AD	Alzheimer's Disease
AF	Ammonium Formate
CNS	Central Nervous System
CT	Computed Tomography
CVD	Cerebrovascular Disease
DAG	Diacylglycerol
DAN	1,5–Diaminonaphthalene
DESI	Desorption Electrospray Ionization
DHB	2,5-Dihydroxybenzoic acid
FLAIR	Fluid-Attenuated Inversion Recovery
FFPE	Formalin Fixed Paraffin Embedded
GM	Monosialo-tetrahexosyl-ganglioside
IMS	Imaging Mass Spectrometry
IP_3	inositol 1,4,5-triphosphate
ITO	Indium Tin Oxide
LMISSD	Lipid MAPS In-Silico Structural Database
MALDI	Matrix-Assisted Laser Desorption/Ionization
MRI	Magnetic Resonance Imaging
MS	Mass Spectrometry
MS/MS	Tandem Mass Spectrometry
m/z	Mass-to-Charge ratio
NAWM	Normal-Appearing White Matter
PC	Phosphatidylcholine
PD	Parkinson's Disease
PE	Phosphatidylethanolamine
PET	Positron Emission Tomography
PG	Phosphatidylglycerol
PI	Phosphatidylinositol
PS	Phosphatidylserine
pvWMH	Periventricular White Matter Hyperintensity
ROI	Region of Interest
SIMS	Secondary Ion Mass Spectrometry
SM	Sphingomyelin
SNR	Signal-to-Noise Ratio
SP	Sphingolipid
ST	Sterol Lipid
TOF	Time of Flight
TrkA	Tyrosine Receptor Kinase A
WMH	White Matter Hyperintensity

CHAPTER 1: INTRODUCTION

1.1. The Brain and Neurodegeneration

The central nervous system (CNS) is responsible for an impressive array of tasks including receiving sensory input, providing motor output, and cognition. The two major components of the CNS are the grey matter, which primarily contains neuronal cell bodies and functions to permit the aforementioned tasks, and the white matter, which is made up of long myelinated neuronal axons and functions to provide communication between grey matter regions and the body. Grey matter and white matter are mutually dependent for proper function, and as such, deterioration of either can result in a myriad of clinical outcomes including chronic disability, decreased quality of life, and death. The societal and economic impacts of CNS diseases cannot be understated as the chronic morbidity of CNS diseases, such as Alzheimer's disease (AD) and Parkinson's disease (PD), means that patients will often require decades of expensive care. Worse yet, morbidity and mortality caused by neurodegenerative diseases will continue to increase with aging populations around the world[1]. For example, AD alone costs an estimated 1% of global GDP and the cost of care is only projected to increase as the global prevalence of AD patients is estimated to surpass 100 million by 2050[2,3]. The severe impacts of CNS diseases, for both the patient and society, makes the research of disease etiology, progression, and treatment imperative to mitigate the impact of CNS diseases.

1.1.2 Neuroimaging

Clinical neuroimaging modalities, such as magnetic resonance imaging (MRI), positron emission tomography (PET), and computed tomography (CT), are invaluable resources for detecting and monitoring CNS disease and injury. MRI is the most

frequently used clinical imaging modality of the CNS and can detect structural abnormalities associated with CNS injury, white matter deterioration, and ischemic events such as stroke[4,5]. Different MRI pulse sequences, most commonly T1 and T2, can be used to alter the visualization of different structures. T2 MRI produces high signal intensity for grey matter and cerebrospinal fluid (CSF), while white matter appears relatively hypointense. T2 MRI combined with fluid-attenuated inversion recovery (FLAIR) is commonly used for neuroimaging of white matter pathologies as FLAIR suppresses the hyperintense signal of CSF thus easing the detection of periventricular white matter abnormalities[6]. Whilst MRI is useful for the detection of CNS diseases in clinical patients, thorough multimodal investigation of MRI-defined post-mortem samples is required for a greater understanding of the molecular mechanisms underlying clinically observable pathologies[4].

1.2. White Matter Hyperintensities

White matter hyperintensities (WMHs) are an early clinical feature of white matter degeneration that can be detected with T2-weighted FLAIR MRI[7–9]. Historically overlooked as an inevitable feature of 'normal aging', recent studies have demonstrated that WMHs are significantly associated with health risk factors and neurodegeneration[10–12]. These WMHs are clinically associated with a 3-fold increased risk of stroke and 2-fold increased risk of dementia[10]. Furthermore, WMHs may contribute to an accelerated rate of global cognitive decline, independent of other neurodegenerative disorders or injury[10]. WMHs are named due to the region appearing bright on MRI relative to the darker signal typically associated with white matter, a change that is attributed to the occurrence of localized edema within the tissue[13]. WMHs are heterogenous in etiology, however,

periventricular WMHs (pvWMHs) are believed to occur in part due to cerebral small vessel disease causing vascular hypoperfusion of the periventricular region resulting in a white matter lesion[14–17]. pvWMHs may be observed to be progressive in routine MRI of patients, a feature associated with a worse neurological prognosis[18,19]. Histological analysis of deteriorated white matter was required to enhance our understanding of the clinically observable feature, however this analysis was delayed due to limitations in detecting white matter deterioration in post-mortem MRI[20,21]. This technical limitation has been ameliorated by improvements in our understanding of MRI signals from formalin-fixed post-mortem samples to the point that post-mortem MRI is now considered to be suitable for designating the spatial extent and severity of WMHs[20].

Numerous studies using post-mortem histopathological analysis of pvWMHs have shown rarefaction of both axons and myelin, as well as an increase of microgliosis and astrocytosis[13,21,22]. Whilst the loss of myelin alone undoubtedly suggests an alteration in the lipid content of these regions, very little is known about specific alterations in the molecular and lipid composition of the tissue underlying pvWMHs. This gap in knowledge is, in part, due to a lack of techniques available for profiling the lipid composition of formalin-fixed post-mortem human brain tissue with adequate sensitivity to resolve differences in the lipid composition of pvWMHs relative to adjacent normal-appearing white matter (NAWM).

1.3 Lipids

Lipids are biological macromolecules that are critical to the function and survival of every cell, but are particularly important for proper function of the CNS. Lipids have incredibly diverse roles, from being constitutive molecules of cell membranes, acting as

energy reservoirs, interacting with a plethora of associated biomolecules to influence their function, and serving as secondary messengers in key cell signalling pathways[23,24]. The functional diversity of lipids is accompanied and accommodated by an even greater diversity in lipid molecular structures, which influence the chemical, physical, and biological properties of lipids[24,25]. This structural and functional heterogeneity contributes to the difficulty of studying lipid expression and distribution within complex heterogenous mixtures, such as human brain tissue, a factor which has delayed our understanding of lipid function. Our understanding of lipid function, while still incomplete, is expanding through the use of multimodal investigations into the diverse mechanisms by which lipids influence cells[26–28]. The technical difficulty of studying lipids within intact biological tissue, has ameliorated with developments in lipid detection techniques, notable imaging mass spectrometry (IMS)[29,30]. Taken together, the critical biological importance of lipids, the historical difficulty of lipid research, and recent advancements in techniques for the study of lipids, have resulted in a unique opportunity to expand our understanding of this understudied trove of biological information.

1.3.1 Lipids in Cell Membranes

The plasma membrane is a dynamic heterogenous bilayer that surrounds every cell, compartmentalizing them from their environment. These membranes were often erroneously characterized from a protein-centric view to be relatively passive barrier that serves to control the flow of molecules and contain the more biologically exciting membrane-proteins[31]. It is becoming increasing recognized that these membranes are heterogeneously composed of diverse lipid species which dramatically influence the

function of the membrane they create, membrane-associated proteins, and the cell as a whole[24].

Our understanding of the complexities and roles of cell membranes has greatly expanded in recent decades. Currently it is recognized that, beside their barrier function, cell membranes are involved in the organization and regulation of numerous cell signalling pathways[23,32]. This organization and regulation can occur via membrane microdomains, previously referred to as lipid rafts, which are small (10-200 nm) regions of the membrane that are heterogeneously enriched in proteins, sphingolipids such as gangliosides, and cholesterol[33–35]. Membrane microdomains are known to undergo dynamic changes in response to the internal conditions and external environment of the cell[34,35]. Interestingly, the lipid component of these membrane microdomains are believed to be potent modulators of the protein composition and signalling pathways associated with these microdomains, such as, ganglioside-mediated regulation of the tyrosine receptor kinase A (TrkA) pro-survival pathway[36,37]. The molecular mechanisms by which lipids influence signaling depending on the pathway in question but include lipid-mediated recruitment of proteins to membrane microdomains and non-covalent lipid-protein binding to alter protein activity[38]. The influence of lipids on protein activity can be exemplified by the ability of specific gangliosides to enhance the activation of the aforementioned TrkA pro-survival pathway, a phenomenon which will be further discussed later in this introduction.

1.3.2 Functions – Structural

The plasma membrane is a complex 3D structure that features incredible biophysical and compositional heterogeneity. It is now known that this heterogeneity,

which occurs both laterally and between leaflets of the bilayer, is not a random phenomenon but rather a complex biophysical system with profound physiological relevance[37]. Alterations in physical membrane properties have been demonstrated influence the activity of transmembrane proteins and peripheral membrane binding proteins which in-turn affect intracellular signalling pathways[23,24]. These physical alterations can be caused by variations in the molecular structures of acyl chains and head groups of lipids. Alterations in these lipid structures influence the physical parameters of the membrane including width, fluidity, and curvature. For example, different lengths and saturations of the acyl chain influence bilayer width, with a longer chain promoting a wider bilayer width[24,39]. According to the widely supported 'hydrophobic mismatch hypothesis', this bilayer width subsequently influences the localization and activity of transmembrane proteins based on the width of their hydrophobic, transmembrane domain (Fig 1A)[39,40].

The tight packing of amphipathic lipids to form a lipid bilayer is an energetic compromise between the hydrophilic and hydrophobic domains, where neither domain exists at the lower energy state they would assume when independent from the other[23]. As such, the lipid bilayer exists as a stable yet highly ordered, high-energy structure. This is driven, in part, by the energetically-favourable association of hydrophilic tails with adjacent tails and results in the crowding of headgroups at the surfaces of the bilayer. The crowding of headgroups means that the structural diversity of headgroups present must be carefully considered when conceptualizing the physical structure of lipid bilayers, as these hydrophilic domains are constantly influencing the adjacent heads with physical and ionic interactions[23,24]. This is demonstrated by the tendency of lipids that contain a

large head group, such as glycosphingolipids, to induce spontaneous positive curvature of a lipid membrane (Fig 1B)[41]. Vice-versa, lipids with a small hydrophilic head, such as PE, tend to induce negative curvature (Fig 1B)[42]. When visualized as a bilayer, the asymmetric distribution of a large headgroup lipid to the outer leaflet and a small headgroup lipid to the inner leaflet would promote intracellular curvature (Fig 1C). The biological relevance of this curvature is demonstrated by the necessity of localized lipid-deacetylation/acetylation enzymes to facilitate golgi membrane fission and other lipid-regulated membrane deformation events[41,43]. While our current understanding of lipid diversity and how it influences the biophysical properties of membranes remains incomplete, lipids play a critical and often understated role in cell function. Continued investigation of lipids and how they influence cell function will undoubtedly assist our understanding and treatment of CNS conditions that include a lipid abnormality component.

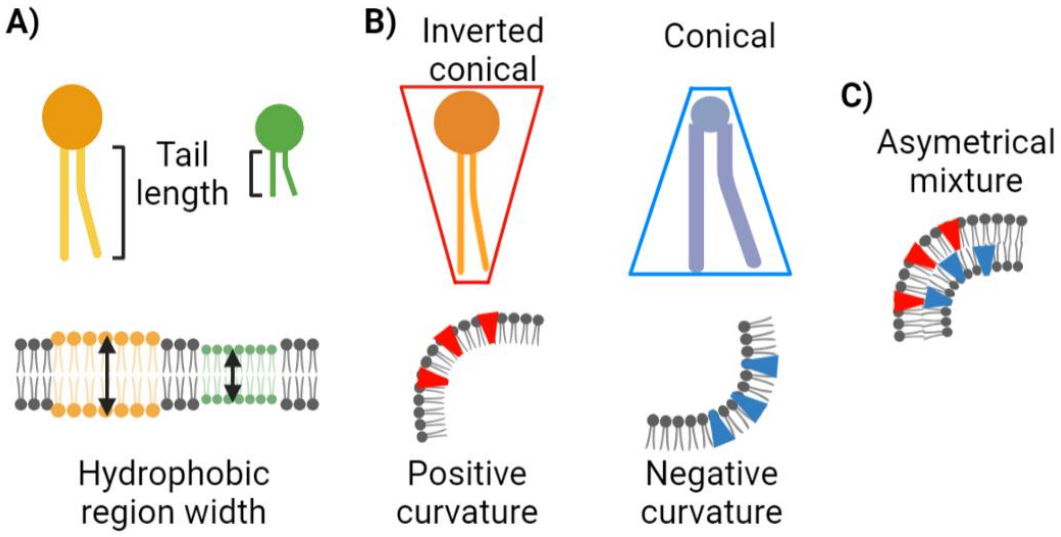

Figure 1. Select examples of the biophysical influence of lipids on lipid membranes. A) Alterations in the length of the hydrophobic tail, influences the width of the hydrophobic region of a lipid bilayer. The alterations in-turn influences the localization of

transmembrane proteins relative to the width of their transmembrane domain. B) The physical structure of the head, and its ratio to tail width, influences lipid membrane curvature. The inverted-cone shape induces spontaneous positive curvature of the membrane. Conical lipids, those with a head width that is narrower than the tail width, induce spontaneous negative curvature of the membrane. C) Asymmetrical bilayer distribution of a conical and inverted-conical lipids can synergistically promote bilayer curvature. Created with Biorender.com.

1.3.3 Functions – Signalling

The mechanisms by which lipids influence cell signalling pathways are multifaceted, a diversity which is required to accommodate the diversity of pathways that are influenced[24]. This diversity, along with the technical difficulties associated with lipid investigation, has impeded our understanding of the mechanisms and functions of specific lipids. Distinguishing the structural and signalling aspects of lipids can be convoluted as lipids can affect signalling indirectly by influencing the physical parameters of the plasma membrane, in-turn influencing membrane-associated signalling pathways. Since some of these structural contributions were previously discussed, this section will instead provide examples of signalling that aren't associated with structural functions, and one interesting example of a structurally-mediated signalling pathway.

One of the most widely known lipid signalling events is the involvement of phosphatidylinositol 4,5-biphosphate (PIP_2) for the transduction and amplification of certain G-protein couple receptor pathways[44,45]. In this pathway, the protein phospholipase C hydrolytically cleaves the head and tail of PIP_2 into the secondary messengers inositol 1,4,5-triphosphate (IP_3) and diacylglycerol (DAG)[45]. The tail, DAG, remains embedded in the inner leaflet of the plasma membrane and goes on to activate members of the protein kinase C family which induce a myriad of downstream effects including proliferation and differentiation[46,47]. Meanwhile the head, IP_3, now liberated from

the membrane can diffuse through the cytoplasm and interact with it's own set of associated pathways, primarily activating channels that induce intracellular release of Ca^{2+}[45,48]. While the downstream signals of DAG and IP_3 can vary depending on cell population and environmental effects, it is clear that these lipid-mediated signalling pathways are essential for proper cell regulation[48]. This is emphasized by the presence of aberrant PIP_2-associated signalling in pathologies such as cancers and AD[48]. In AD, it has been demonstrated that beta-amyloid 42 (Aβ42) oligomers associated with AD can induce intracellular release of Ca^{2+}, which according to the calcium hypothesis of AD is a cytotoxic insult that may contribute to AD pathology[49,50]. This release is believed to be mediated by IP_3, as pre-treatment with IP_3 receptor antagonists attenuates Ca^{2+} release[50]. Interestingly, mass spectrometry (MS) has been used for the detection of PI species, including PIP_2[51,52]. As such, using MS to investigate lipids within pathological tissues may elucidate aberrant PIP_2 signalling if PIP_2 levels were found to be altered within a sample[52].

An interesting structurally-mediated signalling pathway is that of the sphingolipid monosialotetrahexosylganglioside (GM1) and tyrosine receptor kinase A (TrkA). GM1 has been demonstrated to have neurotrophic effects on mature neurons, however the mechanisms for this are uncertain and potentially multimodal[53–55]. One pathway that has been implicated is the TrkA neuronal pro-survival pathway[53]. A current theory postulates that GM1 plays an organizational role, where increased GM1 in the outer leaflet of a plasma membrane encourages the co-localization of TrkA receptors due to interactions between the extracellular carbohydrate moiety of GM1 and extracellular domains of TrkA[56]. TrkA receptors require dimerization for activation, so increased TrkA receptor localization enhances the opportunity for TrkA receptor activation without an increase in

Trk ligands[53]. As such, the organizational properties of lipids such as GM1 may serve as potentiators for associated signalling pathways. Numerous studies have demonstrated robust *in situ* detection of GM1, and associated gangliosides, from brain tissue samples using MS[57,58]. Thus, MS may be able to distinguish ganglioside abnormalities in pathologies, if they exist, which has the potential to guide future investigation of pathways associated with lipid abnormalities and how they relate to the pathology.

1.3.4 The involvement of lipids in diseases of the CNS

The abundance of lipids in the brain, as well as, the aforementioned roles of lipids and lipid metabolites in cell function, means that diseases of the CNS are uniquely prone to have a lipid perturbation component[59]. This is supported by the growing recognition of lipid dyshomeostasis associated with stroke, multiple sclerosis, AD, and Huntington's disease[59–62]. Although some observational studies previously attributed lipids abnormalities to be end-product alterations associated with the disease, recent experimental approaches have demonstrated an active role of altered lipids in mediating disease progression[62,63]. Lipid dyshomeostasis may play a key role in additional diseases of the CNS, however, elucidation of lipid abnormalities has been stymied due to the technical difficulty of specifically and sensitively resolving lipid abnormalities associated with CNS diseases[64]. Furthermore, detection and quantification of lipids while retaining spatial distribution information was historically impossible due to the reliance on techniques that required tissue homogenization[64]. Additionally, tissue homogenization results in the loss of information on lipid alterations that may be specific to distinct cell populations confounding the results of techniques that require homogenization. Expanding our knowledge of lipid abnormalities associated with CNS diseases would

enhance our understanding of potential molecular mechanisms contributing to disease progression, and provide the opportunity for novel lipid-targeting therapeutics[59].

1.4 Mass Spectrometry

MS is a semi-quantitative analytical technique by which a wide variety of molecules such as proteins, lipids, or metabolites in a sample can be detected[65,66]. In general, an MS instrument has three key components, an ion source responsible for the generation of ions from a sample, a mass analyzer which separates ions by their mass-to-charge ratio (*m/z*), and a detector for the subsequent detection of each ion species to generate a mass spectrum[67]. A mass spectrum is an output plot displaying relative ion quantity, known as intensity, on the y-axis with a continuous *m/z* range on the x-axis[67]. This versatile technique permits the simultaneous detection and quantification of a multitude of ionizable molecules, and as such, research has just begun to scratch the surface of the questions which MS can be used to investigate.

1.4.1 Imaging mass spectrometry

IMS is currently the only technique that permits simultaneous *in situ* detection, quantification, and visualization of multiple small molecules, such as lipid species, within a single tissue section[30,66]. IMS functions identically to the mechanism of MS, but the process is repeated in a stepwise manner to generate individual mass spectra for each point on the tissue[68]. This results in the generation of voxels of data, where every pixel in an intensity map of the tissue has an entire mass spectrum contained within it[68]. As such, IMS permits visualization and relative quantification of every detected ion in the mass spectra associated with the scanned sample[68]. The unique ability of IMS to

simultaneously detect, quantify, and visualize multiple ion species makes IMS an invaluable tool for lipidomic studies.

1.4.2 MS Ion Sources

MS relies on the use of ions to separate molecules by their *m/z* and for their subsequent detection by an ion detector. To produce ions from the sample, MS instruments have a critical component referred to as the 'ion source'. Whilst multiple ion sources exist, they are often categorized as 'hard' and 'soft' ionization techniques[69]. In brief, these ion sources differ in how they ionize molecules of interest, however, the differences in ionization influences which molecules are ionized and detected[69]. Hard ionization causes relatively large quantities of energy to be transferred from the ion source to the analyte molecules in the sample, a process which increases the opportunity for fragmentation to occur[69]. In contrast, soft ionization imparts minimal energy to the analytes and risks little to no fragmentation. While hard ionization sources, and the fragmentation that occurs, can be beneficial for analysis in chemically pure samples, fragmentation can confound the mass spectra generated from chemically heterogenous samples, such as tissue samples. For this reason, soft ion sources such as matrix-assisted laser desorption/ionization (MALDI) and electrospray ionization (ESI) are often the preferred technique for tissue analysis[69,70]. As such, careful consideration and selection of an ion source is an important facet of planning any MS experiment. The following subsections will provide a brief discussion of ion sources in the context of lipidomic investigations.

An additional consideration regarding the detection of lipid ions in MS is that lipid ions display preferential negative or positive ionization depending on the composition of

their headgroup[30]. As a generalization, negative ion detection scans of human brain tissue tend to detect $[M-H]^-$ ions of phosphatidylethanolamines (PE), phosphatidylserines (PS), phosphatidylinositols (PI) and acidic sphingolipids[30]. In-contrast, positive ion detection spectra of brain tissue are dominated by sphingomyelins (SM) and phosphatidylcholines (PC), the latter of which are often detected in such abundance that the detection of other lipid species is suppressed[30,71]. This abundance of PC and SM species is due to their quaternary amine group which contains a permanent positive charge[30]. Whilst negative lipid ions tend to form as $[M-H]^-$, positive lipid ions commonly form as $[M+H]^+$, $[M+Na]^+$, $[M+K]^+$[30]. While these assumptions can help when beginning to interpret a MS dataset, it must also be considered that other ions exist, such as the dehydration of cholesterol to form the commonly detected *m/z* 369.3 $[cholesterol-H_2O]^+$ ion[72]. As such, the variety of possible ions must be careful considered when analyzing any dataset, a possibility which can be added by additional MS techniques discussed later.

1.4.3 Ion sources - ESI

ESI has been used as a soft ion source for biomolecules since the 1980s, however, this technique has several limitations when working with complex heterogenous mixtures such as biological samples[73,74]. The process of ESI involves the introduction of a solvent, evaporation, and development of distinct gas-phase ions[75]. A key difference between MALDI and ESI is that the process of ionization in ESI occurs with a liquid-phase to gas-phase transition, in contrast to the solid to gas-phase transition of MALDI. This requirement for a liquid-phase sample means that ESI is incompatible with IMS, as introduction of a solvent produces in homogenization and loss of spatial information prior to ionization. Additionally, ESI is susceptible to contamination from salts and other

endogenously occurring molecules in biological samples[76]. These contaminants must be separated from the sample using liquid chromatography prior to ionization. Lastly, ESI is prone to producing ions with multiple charges[73]. This phenomenon can be beneficial for the analysis of large biomolecules, such as proteins, as most MS instruments function best for the detection of molecules in the <1500 *m/z* range[67]. However, the majority of lipids already occur with a mass of <1500 Daltons and as such do not require multiple charges to be detected in the <1500 *m/z* range[72]. Furthermore, the addition of multiple charges risks a loss of mass resolution as each additional charge halves the *m/z* difference of ions of different masses. The limitations of ESI regarding analysis of biological samples, lipid detection, and incompatibility with IMS, necessitated the development of further soft ionization sources.

1.4.4 Ion sources - MALDI

MALDI is a commonly used ion source for lipidomic investigations due to its 'soft ionization' process, meaning that relatively little energy is imparted into the molecule to generate an ion. Soft ionization is essential for lipid detection experiments as it reduces the risk of fragmentation occurring, a process that can confound lipid studies as fragments of larger lipid species are often indistinguishable to intact molecules of smaller related lipids[77]. The soft ionization of MALDI is achieved by coating the sample with the desired matrix, which infiltrates the sample to form crystals around molecules and assists in the transfer of energy from a laser pulse to the molecules of interest[78] (Fig 2). This laser pulse heats a localized spot to energetically excite the matrix, resulting in the molecules within undergoing a gas-phase transition and ionization. While the mechanism of ionization remains uncertain, the dominant theory is gas-phase ionization where the analyte

molecules are protonated or deprotonated by surrounding gas-phase matrix ions[78,79]. Depending on the matrix chosen MALDI can be suitable for the ionization and detection of a variety of biomolecules, including proteins, carbohydrates, and lipids[80]. Due to the diversity of molecules that can be detected, the reduced risk of delocalization, and the minimal fragmentation induced by soft ionization, MALDI was chosen as the ion source for the experiments discussed in this work.

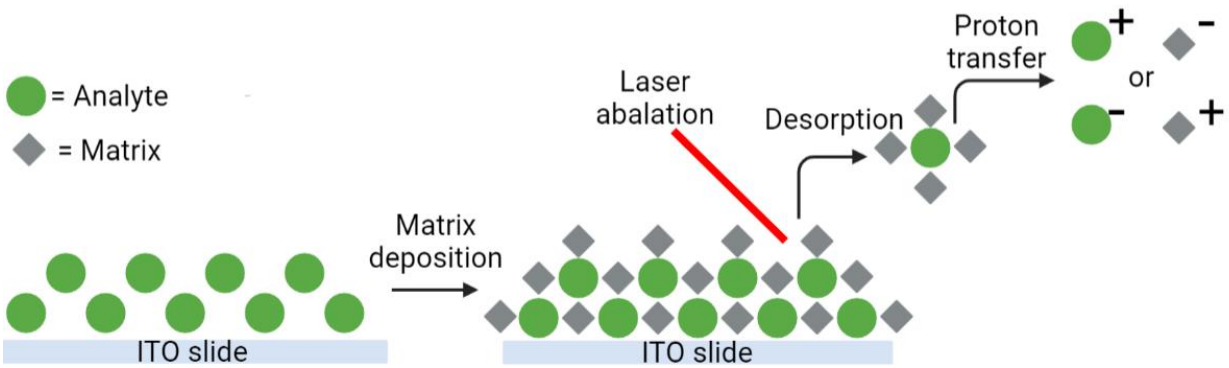

Figure 2. Schematic of the process of matrix deposition, desorption, and ionization in MALDI MS. Following matrix application, matrix molecules co-crystalize with analyte molecules. Upon laser ablation, the matrix assists the gentle transfer of heat energy from the laser to molecules within the sample. This energy permits the desorption transition into gas phase, as well as proton transfer to or from the analyte molecules to ionize them for subsequent TOF and detection. Created with Biorender.com.

1.4.5 Limitations of MALDI

Limitations of MALDI as an ion source include concerns about reproducibility due to heterogenous matrix application and the semi-quantitative nature of ion detection from a heterogenous sample[30]. Fortunately, both limitations can be ameliorated by methodology. Homogenous matrix application can be achieved by matrix sublimation/deposition, a process which involves heating a known mass of solid-phase matrix inside a vacuum chamber to induce sublimation, solid to gas-phase transition[81]. As the gas-phase matrix diffuses through the chamber it contacts the sample mounted to

a slide which has been conductively cooled by an ice slush chamber above. This temperature difference causes deposition, gas to solid-phase transition, homogenously across the sample. Although matrix application can be improved by the use of matrix sublimation, the semi-quantitative nature of MALDI MS, is far more difficult to overcome. Quantification limitations are due to spectrum saturation from the most prevalent ions and uncertainties in the mechanism of ionization for each matrix[82]. In a complex biological sample, it is unlikely that absolute quantification can ever confidently be achieved, as such, it is best to use MALDI IMS for relative intrasample comparison of detected ions, or inter-sample comparison of similar tissues that have been identically prepared.

1.4.6 Mass analyzers

As previously mentioned, mass analyzers are a critical component of any MS instrument, responsible for the separation of ions by their *m/z*. While various mass analyzers exist, they typically function by using charged fields to control the movement of gas-phase ions produced from the sample. As with other facets of the MS instrument, selection of a mass analyzer should be unique to each experiment. This is due to differences in the three key characteristics of mass analyzers; mass accuracy, the accuracy of experimental *m/z* values to actual *m/z* values, mass resolution, the *m/*z limit at which the analyzer can distinguish two mass peaks, and mass range, the range, and limits of *m/z* values that an analyzer can be used for[83]. Commonly used mass analyzers include time-of-flight (TOF), quadrupole, and quadrupole ion trap. Detailed discussion of the types of mass analyzers and their mechanisms exceeds the scope of this introduction, but several in-depth reviews on the topic exist[83,84].

1.4.7 Time-of-flight mass analyzers

TOF is a commonly used mass analyzer due to its rapid mass spectrum acquisition speed, and high mass accuracy, mass resolution and mass range[83]. In a MALDI-TOF-IMS instrument, TOF occurs following MALDI when analyte molecules have already undergone gas phase transition and ionization (Fig 3A). The analyte ions are passed through a series of magnetically charged gates causing them to accelerate through a flight tube. This flight tube serves to separate analyte ions based on both their mass and charge since heavier molecules will fly slower than lighter molecules of identical charge. At the end of the flight tube a detector measures both the time is takes for ions to arrive, which permits the assignment of *m/*z values to these ions, and the quantity of ions arriving at a given *m/z*, allowing the user to semi-quantitatively interpret the number of ions generated from a sample. Due to the benefits of TOF, such as rapid acquisition of broad mass spectra, TOF mass analyzers are particularly suited for lipidomic investigations.

1.4.8 Ion identification and MALDI TOF/TOF tandem mass spectrometry

Ion identification is a necessary part of any MS experiment, and can be a particularly difficult task in untargeted, shotgun-style analysis of molecularly-complex samples such as human tissue[30]. Ion identities can be assigned by accurate mass, by which the experimental *m/z* value is compared to theoretical *m/z* values, however, this approach is limited by both the mass accuracy of the instrument and the inability to distinguish ions of identical *m/z* such as structural isomers which commonly occurs with lipids[30,72]. As such, tandem mass spectrometry (MS/MS) is the gold-standard for identification of ions detected in MS experiments[30,72]. MS/MS differs from standard MS by coupling two mass analyzers in sequence (Fig 3B). This permits the selection of ions detected at a specific *m/z* value in the first mass analyzer, annotated as MS^1, causing all

other ions to be gated out of the second mass analyzer, MS^2. Before the selected ions, known as precursor ions, reach MS^2, they are subjected to fragmentation into product ions, which enables the production of a 'fingerprint-like' mass spectrum at MS^2 based on the *m/z* of each product ion fragment. The product ion fragments that a molecule can produce are often predictable based on its molecular structure and its innate tendency to fragment at certain bonds[85]. A prime example of this is the tendency for the lipid head group, or a portion of it, to fragment away. This headgroup fragment alone can dramatically assist lipid identification by indicating the lipid class from which parent ion originated (Table 1). MS/MS is an invaluable identification technique for heterogenous samples that contain many distinct molecules occurring at similar *m/z* ranges, such as lipids in human brain tissue.

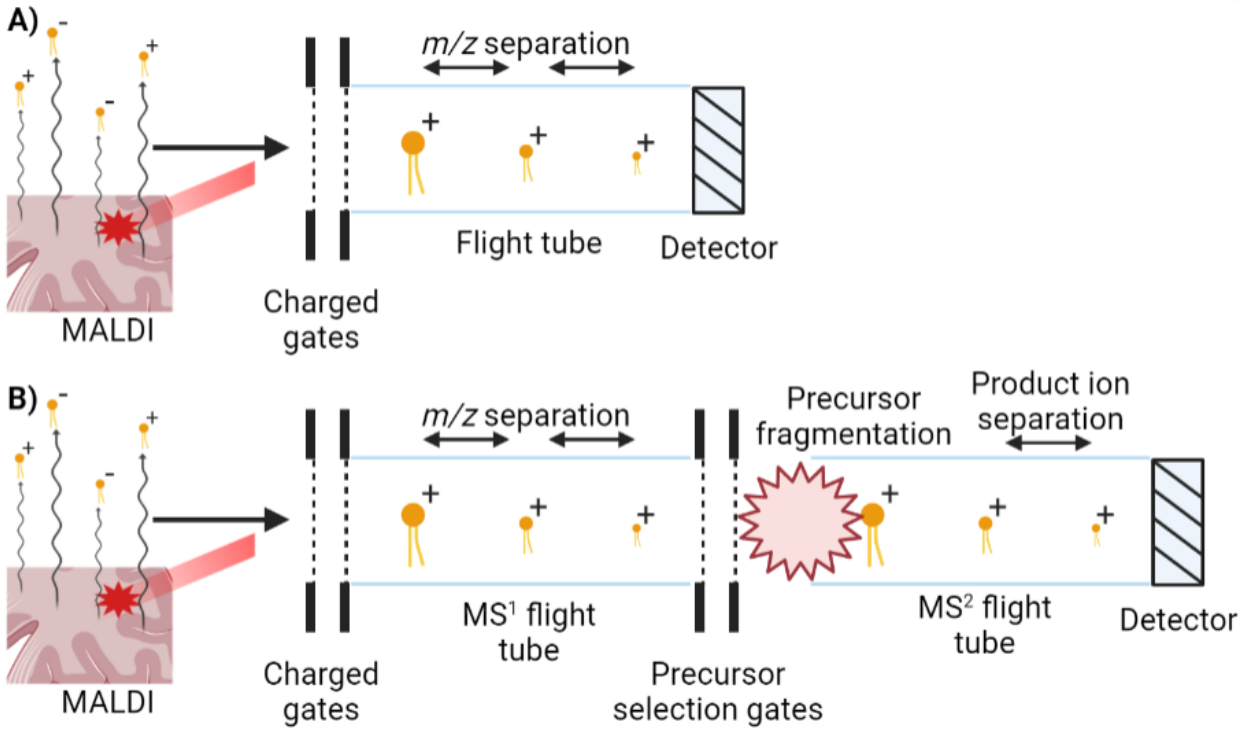

Figure 3. Schematic of mass analysis by TOF and TOF/TOF MSMS following MALDI. A) Following MALDI, gas phase ions are accelerated into a flight tube by a potential difference between the sample plate and a series of charged gates. Molecules of identical charge receive the same amount of kinetic energy, causing heavier molecules to fly slower than lighter molecules of the same charge. This separation of molecules based on their *m/z* as they move through the flight tube causes them to reach the detector at different times which assigns an *m/z* value to each molecule based on its relative arrival time. B) TOF/TOF MSMS is achieved by connecting two TOF mass analyzers in sequence. This permits the selection of molecules at a given *m/z* by gating other molecules out of the second analyzer. Selected molecules then undergo fragmentation, and the product ions of the precursor species are subjected to TOF and subsequent fragment analysis for precursor identification. Created with Biorender.com.

Lipid Category	Product Ion *m/z*	Product Ion Identity
General phospholipids	79	[phosphate-H]$^-$
	153	[glycerol phosphate-H_2O-H]$^-$
	171	[glycerol phosphate-H]$^-$
PE	196.0	[Phosphoethanolamine-H_2O-H]$^-$
	M-43	[Precursor-ethanolamine]$^-$
PI	241	[Inositolphosphate-H_2O]$^-$
PS	M-87	[Precursor-serine]$^-$
Acidic glycosphingolipids (Gangliosides)	290	[N-acetylneuraminic acid-H]$^-$

Table 1. Summary of characteristic lipid fragments observed in negative mode MSMS. Summary of characteristic lipid fragments previously observed in MSMS product ion spectra generated from lipids. Relevant citations for all ion species are in the main text.

1.4.9. MALDI IMS of lipids

Historically, technical limitations prevented detection and quantification of lipids while maintaining both spatial distribution and lipid species specificity. This is due to techniques relying on either immunohistochemistry, which maintains spatial distribution but loses specificity for the hydrophobic domain, or analysis of extracted homogenized tissue which causes loss of spatial distribution information[72]. Throughout the 1990s and 2000s this barrier was breached by the application of MALDI IMS for in situ detection of biomolecules[86,87]. Since then, MALDI IMS has been applied for the detection of diverse lipid species within numerous human tissues including brain, liver, and various tumours. In these tissues, MALDI IMS has detected sub-classes of phospholipids and sphingolipids (SP), such as PCs, PIs, and gangliosides, which are known to influence cell function and

survival[82]. As such, detection of these lipids within a sample can improve our understanding of molecular pathways occurring within the sample.

An interesting application of MALDI IMS is for the elucidation of regional lipid abnormalities within a tissue sample, as shown by the detection of lipid disturbances in pathological tissues such as stroke injuries[60]. This application of MALDI IMS allows for *in situ* detection, visualization, and quantification of multiple lipid species within a sample, allowing for a lipidomic-level approach to identifying differences between pathological regions and adjacent healthy regions within a single sample. Such an approach can be used for either experimental investigation or diagnostically. Work within this thesis will focus on the use of MALDI IMS for experimental investigation of tissues and their lipid profiles. The investigative application of MALDI IMS for distinguishing regional lipid abnormalities has previously identified abnormalities in diverse lipid classes such as PCs, PIs, PEs, and SP. These studies enhance our knowledge of the molecular mechanisms that underlie pathologies and provide novel treatment avenues by identifying dysregulated lipids that may be targeted to ameliorate disease progression.

1.4.10 Tissue preservation and MALDI IMS

Post-mortem tissue preservation is a critical step to maintain morphological and molecular fidelity. These post-mortem alterations, which begin to occur within minutes, are most commonly prevented by chemical-fixation with formalin, formaldehyde, or paraformaldehyde which prevent post-mortem deterioration, in part, by cross-linking proteins to prevent their enzymatic activity[88]. Chemical-fixation techniques are commonly used due to the ease of the preservation protocol and samples not requiring expensive cold storage[88]. As such, robust tissue banks containing chemically-fixed samples with

clinical associations have been developed for post-mortem analysis. However, the gold-standard tissue for MALDI MS has long been fresh-frozen tissue, tissue which is snap-frozen soon after extraction[58,89]. Indeed, MALDI MS was previously believed to be incompatible with formalin-fixed tissue, largely due to fixation causing the cross-linking of proteins and the concerns that fixatives inhibit the detection of lipid molecules[58,89]. While fixatives may inhibit the detection certain lipid classes, such as PEs, recent studies have demonstrated that detection of both proteins and lipids from formalin-fixed archive tissue is possible with MALDI MS[58,89,90]. As such, numerous archived formalin-fixed clinically-relevant tissue samples can now be investigated using MS to elucidate molecular abnormalities associated with pathologies.

1.5 Rationale

Lipids play a critical and dynamic role in regulating cell function and survival. Lipid abnormalities observed in various pathologies, such as AD, stroke, cancers, and multiple sclerosis, are now known to play a role in disease progression. Whilst lipid abnormalities have been observed in some CNS diseases, the technical limitation of lipid detection in clinically-relevant formalin-fixed human archival tissue has prevented a greater understanding of specific lipid species alterations. MALDI IMS is a molecular imaging technique that permits untagged, *in situ* quantification and visualization of a variety of molecules, including multiple lipid classes. To our knowledge, MALDI IMS has never previously been applied to distinguish regional lipid abnormalities within MRI-defined formalin-fixed post-mortem human brain tissue. Combining current clinically relevant imaging techniques, such as MRI, and lipidome analysis with MALDI IMS will permit the identification of regional lipid abnormalities associated with pathologies. By elucidating regional lipid abnormalities, we will better understand clinically observable neurological features, disease mechanisms, and progression, as well as provide novel lipid-based targets for therapeutic intervention.

1.6 Aim and Hypothesis

Aim: Investigate the application of MALDI IMS for unbiased, shotgun-style investigation of neuroanatomical-specific lipid abnormalities within MRI-defined, post-mortem, formalin-fixed human CNS tissue.

Hypothesis: Lipid abnormalities exist within pathological white matter regions identified using post-mortem T2-weighted FLAIR MRI, and MALDI IMS can resolve these abnormalities relative to adjacent normal-appearing white matter.

CHAPTER 2: METHODS

2.1 Specimen Selection for MRI Imaging

Specimen for MRI imaging were chosen based on neuropathological findings documented by a certified Neuropathologist at autopsy. Intact brains were obtained from a bank of samples that had been stored in 10% neutral buffered formalin for up to 15 years following previous neuropathological examination. One coronal slice from the frontal lobe of each specimen was selected for imaging. The final selection for MRI imaging included 20 specimens. Demographic data for the 20 specimens can be found in Supplementary Table 1.

2.2 MRI Brain Imaging

All scans were performed at Robarts Research Institute's Centre for Functional and Metabolic Mapping on a MAGNETOM 7T MRI Scanner (Siemens). Coronal slices of fixed tissue from the frontal lobes of the brain were removed from formalin and immersed in Galden HT-270 perfluorinated fluid (Kurt J Lesker Company, Vaughan, ON, Canada). 5 coronal sections were scanned simultaneously using a custom-made stacking device until coronal sections from all 20 specimens were scanned. The stacking device was secured into the head coil apparatus for scanning. Structural MRI images were acquired in the coronal orientation with the following sequences: 3D T1-weighted MPRAGE (1 mm slice thickness, TR/TE=3000/1.72 ms, flip angle =90, FOV= 160 x 126 mm , in-plane resolution of 0.7 x 0.7 mm), 3D T2-weighted SPACE sequence (1mm slice thickness, TR/TE=2500/349 ms, flip angle= 90 FOV = 160 x 120 mm, in plane resolution of 0.5 x 0.5 mm) and 3D FLAIR sequence (1mm slice thickness, TR/TE/T1=8000/205/1600 ms, flip angle= 90, FOV= 160 x 120 mm, in-plane resolution of 0.63 x 0.63 mm).

2.3 Specimen Selection for MALDI TOF IMS Scanning

PvWMHs from the cohort of MRI-scanned specimens were qualitatively evaluated using a modified version of the Fazekas' rating scale[91]. Eleven brain specimens were selected for MALDI TOF IMS imaging that met the MRI-criteria for "moderate pvWMH", which involved a lesion that extended greater than 1/3 of the distance between the edge of the ventricle and the cortex. Nine of these brain specimens had bi-lateral moderate periventricular WMHs, the remaining two brain specimens were scored as moderate periventricular WMH for only one hemisphere. As such, a total of 20 distinct moderate pvWMHs from 11 brain specimens were selected for MALDI TOF IMS scanning. These specimens represent a heterogenous group with neuropathological diagnoses of Alzheimer's disease and/or cerebrovascular disease. Remaining specimens from the MRI-scanned cohort were excluded due to an evaluation of less than or more than "moderate pvWMH" on the modified Fazekas' ratings scale.

2.4 Tissue blocking

Tissues containing periventricular white matter were sampled for tissue selection based on MRI findings. Tissue blocks were obtained from brain tissue that included the moderate pvWMH, subcortical white matter and cortical tissue. Block were stored in 10% neutral buffered formalin prior to processing. The anatomy of the cortex and subcortical structures was used to correctly match the tissue to the corresponding MRI image.

2.5 Tissue Sectioning and Mounting

Formalin-fixed non-embedded tissue blocks were sectioned at 10 µm thickness using a Cryostar NX50 cryostat (Thermo-Fisher Scientific, Toronto, ON, Canada) at -

25°C. Tissue sections were then thaw-mounted to electrically conductive indium-tin-oxide coated slides (Hudson Surface Technology Inc., Old Tappan, NY, USA).

2.6 Ammonium Formate Wash

Ammonium formate (AF) washes were performed to enhance lipid signal from formalin-fixed tissue as previously described[58].

2.7 Matrix Sublimation

Mounted tissue sections were placed into a sublimation apparatus (Chemglass) for sublimation with either DAN matrix (Sigma-Aldrich, Oakville, ON, Canada) for negative ion mode scans or DHB matrix (Alfa Aesar, Haverhill, MA, USA) for positive ion mode scans. Assembly of apparatus and sublimation of DAN[57] and DHB[92] was performed as previously described.

2.8 MALDI-TOF-IMS

MALDI TOF IMS was performed using a Sciex 5800 TOF/TOF system, MALDI TOF/TOF (Sciex, Framingham, MA, USA) equipped with a 349 nm Nd:YLF OptiBeam On-Axis laser using a laser pulse rate of 400 Hz as previously described[58]. Reflectron negative scans were conducted from *m/z* 450-1000 and *m/z* 1000-2000. Reflectron positive scans were conducted from *m/z* 450-1000. TOF TOF Series Explorer (Sciex) and Data Explorer (Sciex) software were used for data acquisition and processing, respectively.

2.9 Image and Data Analysis

MALDI IMS data was visualized using TissueView software (Sciex). Manual selection of Region of Interests (ROIs) in white matter that appeared normal on MRI (NAWM), and periventricular white matter that appeared hyperintense with MRI (pvWMH)

was performed through co-visualization of MALDI TOF IMS images and reference MRI scans. Average mass spectra per ROI were then simultaneously generated for each ROI. Mass peaks were acquired from each mass spectra based on our established criteria of a minimum signal-to-noise ratio (SNR) >3. Mass peaks that did not meet the SNR criteria were omitted. Mass peaks were assessed for consistent detection (>80%) in scans from all 21 tissue blocks. Mass peaks which were consistently detected in >80% of scans were carried forward for statistical analysis. Intensity values corresponding to the monoisotopic peak of consistently detected mass peaks were isolated for intrasubject comparison.

2.10 Identification of Lipid Ions by Searching Experimental m/z in LMISSD and SwissLipids

Identification of mass peaks was primarily conducted by using experimental *m/z* values to interrogate the LIPID Metabolites and Pathway Strategies (MAPS) In Silico Structural Database (LMISSD)[93]. A second independent database, SwissLipids, was interrogated using the same approach. Database searches were conducted with the following parameters:

Experimental *m/z* searches of mass peaks detected in negative ion mode:

Mass Tolerance (*m/z*): ± 0.1

Ion Adducts: $[M-H]^-$

Experimental *m/z* searches of mass peaks detected in positive ion mode:

Mass Tolerance (*m/z*): ± 0.1

Ion Adducts: $[M+H]^+$, $[M+Na]^+$, $[M+K]^+$

LMISSD resource available at:

https://www.lipidmaps.org/resources/databases/lmissd/search.php.

SwissLipids resource available at:

https://www.swisslipids.org/#/advanced

2.11 Identification of Previously Unidentified Mass Peaks by MALDI TOF Tandem Mass Spectrometry

To assist the identification of select mass peaks in negative low-range, tissue was prepared for MALDI TOF IMS imaging and subjected to tandem mass spectrometry (MSMS) in the Sciex 5800 TOF/TOF system, MALDI TOF/TOF (Sciex, Framingham, MA, USA). Reflectron negative mode was used to generate negative MSMS from parent peaks in the *m/z* 450-1000 range and *m/z* 1000-2000 range. Reflectron positive mode was used to generate positive MSMS from parent peaks in the *m/z* 450-1000 range. Reflectron modes were externally calibrated at 50 ppm mass tolerance and internally at 10 ppm mass tolerance. TOF/TOF Series Explorer (Sciex) and Data Explorer (Sciex) software were used for data acquisition and processing respectively. MSMS product ion spectra were visualized using LipidBlast[85]. MSMS search criteria were set using the previously described recommendations[85]. Manual interrogation of MSMS product ion spectra was performed to identify the presence of characteristic lipid class peaks.

2.12 Statistical Analysis

Intrasubject lipid comparison was conducted by comparing monoisotopic intensity values of NAWM to pvWMH for every mass peak that was detected in >80% of the 21 tissue blocks scanned. Paired two-tailed Student's t-tests were used to test for

significance between NAWM and pvWMH for each mass peak. A p-value of <0.05 was considered significant. N indicates biological N-value.

CHAPTER 3: RESULTS

3.1 Lipid Detection Metrics

Analysis of MALDI IMS spectra from all 21 tissue blocks yielded a total of 87 unique ions in negative ion high-range scans, 125 unique ions in negative ion low-range scans, and 96 unique ions in positive ion low-range scans (Table 2). These mass peaks were then assessed between for consistent detection in all specimens (observed in >80% of the 21 tissue blocks). A total of 30 ions from negative ion high-range scans, 41 ions from negative ion low-range scans, and 45 ions from positive ion low-range scans were carried forward for statistical evaluation.

Scan Mode	Total Ion Species	Ion Species with >80% Detection
Negative ion *m/z* 1000-2000	87	30
Negative ion *m/z* 450-1000	125	41
Positive ion *m/z* 450-1000	96	45

Table 2. MALDI IMS of formalin-fixed post-mortem human white matter consistently detected 116 ion species. Peaks detected in mass spectra generated using a Sciex 5800 TOF/TOF system, from post-mortem human brain tissue using Reflectron negative and positive ion modes with DAN and DHB matrices, respectively.

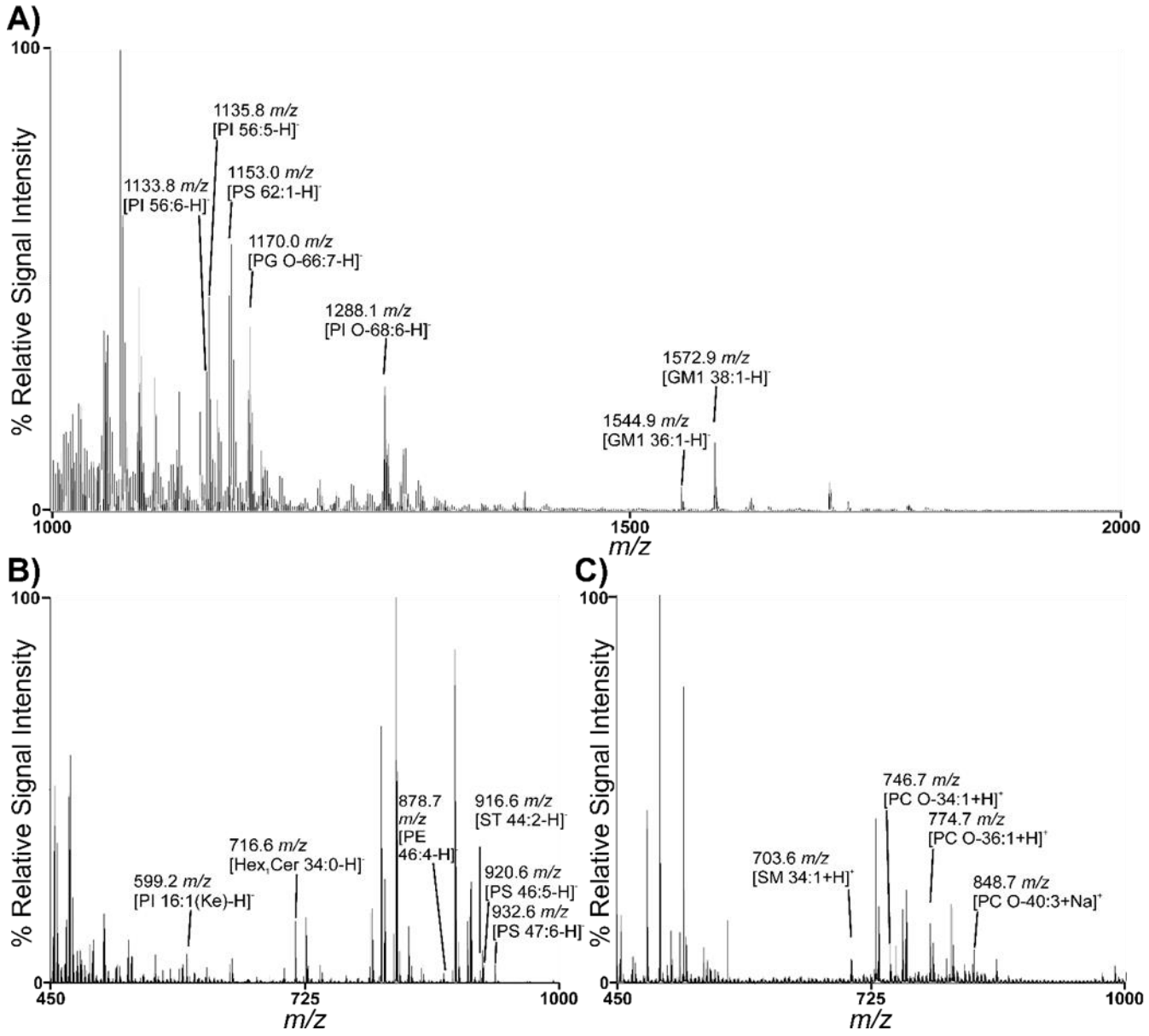

Figure 4. Annotated MALDI-TOF mass spectra of post-mortem human white matter. Representative white matter mass spectra annotated with tentative lipid ion identities for mass peaks that were significantly altered between pvWMH and NAWM. A) Negative ion mass spectrum *m/z* 1000-2000 obtained from tissue sublimated with 1,5-DAN matrix in negative ion detection mode. B) Negative ion mass spectrum *m/z* 450-1000 obtained from tissue sublimated with 1,5-DAN matrix in negative ion detection mode. C) Positive ion mass spectrum *m/z* 450-1000 obtained from tissue sublimated with 2,5-DHB matrix in positive ion detection mode.

3.2 Negative ion MALDI IMS scans detect regional lipid abnormalities within pvWMHs – m/z 1000-2000 Range

Intrasubject comparison of negative ion spectra at *m/z* 1000-2000 elucidated significant differences in 10 of the 30 mass peaks assessed (Fig. 5, Table 1). An increase of monoisotopic peak intensities in the pvWMH relative to NAWM were observed for the ion species occurring at *m/z* = 1572.9 and 1544.9 (Fig. 5). Decreases in monoisotopic peak intensities were observed for the ions at *m/z* = 1303.1. 1288.1, 1170.0, 1153.0, 1135.8, 1133.8, 1110.8, and 1108.8 (Fig. 5).

Identities were assigned to lipid ions by searching two independent lipid databases, LMISSD and SwissLipids, with experimentally generated *m/*z values using the parameters described in our methods (Fig. 5, Table 3). This method for identity assignment often yielded multiple tentative identities that were indistinguishable at MS^1, as such, on-tissue MALDI MSMS was performed to assist in lipid class assignment. We attempted to generate MALDI MSMS product ion spectra from all significantly different mass peaks, however, not all mass peaks produced conclusive MALDI MSMS product ion spectra. MALDI MSMS product ion spectra were manually interrogated for the presence of characteristic fragments to assist confident assignment of lipid class, a similar approach taken by previous untargeted MALDI MS investigations[87]. Detailed structural characterizations of select product ion spectra, such as from the precursor occur at *m/*z = 1544.9 (Fig. 6), were performed, however complete characterization of all species is beyond the scope of the current investigation.

All product ion spectra generated from precursors detected in negative high-range scans, excluding the precursor ions occurring at *m/z* = 1572.9 and 1544.9, produced fragment ions at either *m/z* = 153, 171, or both (Table 3). These product ion fragments

correspond to [glycerol phosphate-H_2O-H]$^-$ and [glycerol phosphate-H]$^-$, respectively, as such, precursor ions that fragment to produce these product ions can be unambiguously identified as glycerophospholipids (Table 1, 3).

Following unambiguous confirmation that all significantly altered species, excluding the precursor ions occurring at *m/z* = 1572.9 and 1544.9, were in fact glycerophospholipids, lipid class assignment was attempted by manually assessing product ion spectra for the presence of characteristic fragments. Table 1 provides a summary of previously published characteristic lipid fragments that may be observed in negative mode product ion spectra generated from major lipid classes detectable using MALDI IMS in human brain tissue[30,94–96]

The product ion spectra of the precursor ions occurring at *m/z* = 1572.9 and 1544.9 both contained prominent fragment peaks at *m/z* = 290.0, a characteristic fragment of gangliosides which corresponds to [N-acetylneuraminic acid-H]$^-$ (Table 1, 3)[58]. Detailed structural characterization of the precursor ion occurring at *m/z* = 1544.9 was performed using the MALDI MSMS product ion spectra (Fig. 6). The presence of the [N-acetylneuraminic acid-H]$^-$ fragment supports the confident assignment of monosialoganglioside (GM) species [GM1 38:1-H]$^-$ (d20:0) and [GM1 36:1-H]$^-$ (d18:0) to *m/z* = 1572.9 and 1544.9, respectively, as has been identified in previous publications[97].

Our experimental *m/z* value for the species occurring at *m/z* 1303.1 failed to provide reliable identification in either lipid database used. Analysis of the MALDI MSMS product ion spectra from this peak was inconclusive, possibly due to the low SNR of the precursor. However, product ion peaks were observed at *m/z* 97.0 and 171.0, known

phospholipid headgroup fragments, confirming that the ion occurring at *m/z* 1303.1 is a phospholipid of unknown identity.

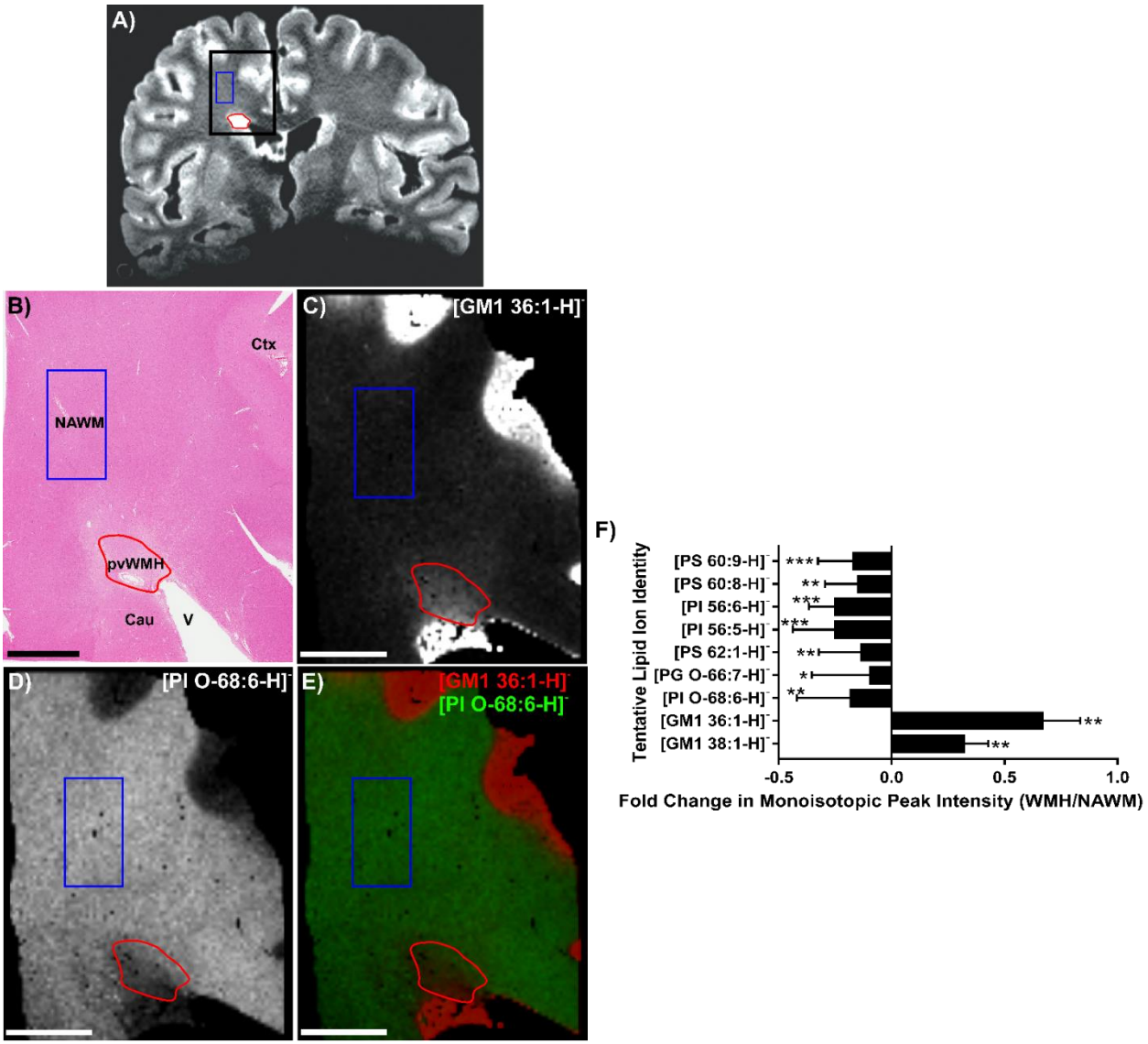

Figure 5. High range negative ion detection MALDI IMS scans distinguished increased and decreased lipid ion intensity in pvWMHs relative to NAWM in post-mortem human tissue. A) Coronal FLAIR MRI of a post-mortem human brain. Red asterisk indicates region identified as a pvWMH. Black box indicates approximate area that was dissected for sectioning. Red outline indicates extent of pvWMH. Blue outline indicates a region of NAWM. B) H&E. V, Cau, and Ctx indicate ventricle, caudate, and cortex, respectively. Scale bar = 5 mm. C) & D) MALDI IMS scans conducted on post-mortem human brain tissue sublimated with 1,5 DAN matrix. Intensity maps generated from (C) $[GM1\ 36:1\text{-}H]^-$ and (D) $[PI\ O\text{-}68:6\text{-}H]^-$. Scale bars = 5 mm. E) Pseudocoloured intensity maps showing the overlay of $[GM1\ 36:1\text{-}H]^-$ and $[PI\ O\text{-}68:6\text{-}H]^-$. F) pvWMH:NAWM fold-change of monoisotopic peak intensity for statistically significant

lipids. Data presented as mean(SD). * indicates p<0.05,**p<0.01, ***p<0.001 via two-tailed Student's T-Test (n=18-20).

Experimental *m/z*	Product Ion *m/z* (MSMS)	Tentative Identification	Theoretical *m/z*	Mass Error (ppm)
1572.8999	87.0, 154.0, 289.9, 790.3, 916.9, 1283.7	[GM1 38:1-H]$^-$ (d20:0)	1572.9007	-0.5073
1544.8690	87.0, 154.0, 290.0, 561.8, 726.6, 790.3, 888.5, 1254.0	[GM1 36:1-H]$^-$ (d18:0)	1544.8694	-0.2466
1303.0667	97.0, 171.0, 435.4, 663.9, 793.9, 1171.1, 1234.8	Unidentified	N/A	N/A
1288.0513	87.0, 153.0, 171.0, 435.3, 496.2, 669.5, 795.9, 951.0, 1206.0	[PI (O-68:6)-H]$^-$	1287.9807	54.8146
1169.9988	97.0, 153.0, 171.0, 281.2, 433.3, 644.3, 723.9, 989.6	[PG 64:0-H]$^-$	1170.0033	-3.8795
1152.9863	78.9, 153.0, 171.0, 281.2, 456.8, 569.5, 699.0, 798.4, 1096.0	[PS 62:1-H]$^-$	1152.9516	30.1062
1135.8073	153.0, 171.0, 255.2, 281.3, 435.3, 620.1, 882.9, 935.7	[PI 56:5-H]$^-$	1135.8159	-7.6262
1133.7919	153.0, 171.0, 226.0, 409.2, 686.3, 694.9, 728.6, 936.8	[PI 56:6-H]$^-$	1133.8003	-7.4025
1110.8079	153.0, 171.0, 401.2, 459.1, 684.6, 743.9, 783.8, 790.3, 797.6, 889.2 931.7	[PS(60:8)-H]$^-$	1110.8108	-2.6107
1108.8065	153.0, 171.0, 417.2, 649.6, 686.4, 740.1, 790.6, 905.0	[PS(60:9)-H]$^-$	1108.7951	10.2814

Table 3. Identification of significantly altered lipid ions detected in negative ion high-range scans by database interrogation and negative mode on-tissue MALDI MSMS in formalin-fixed post-mortem human white matter. Peaks detected in mass spectra generated using a Sciex 5800 TOF/TOF system, from DAN-coated post-mortem human brain tissue in negative ion mode at *m/z* 1000 – 2000. Theoretical *m/z* values and identification based on experimental *m/z* searches in LMISSD and SwissLipids, complemented with manual interrogation of on-tissue MALDI MSMS as described in Methods.

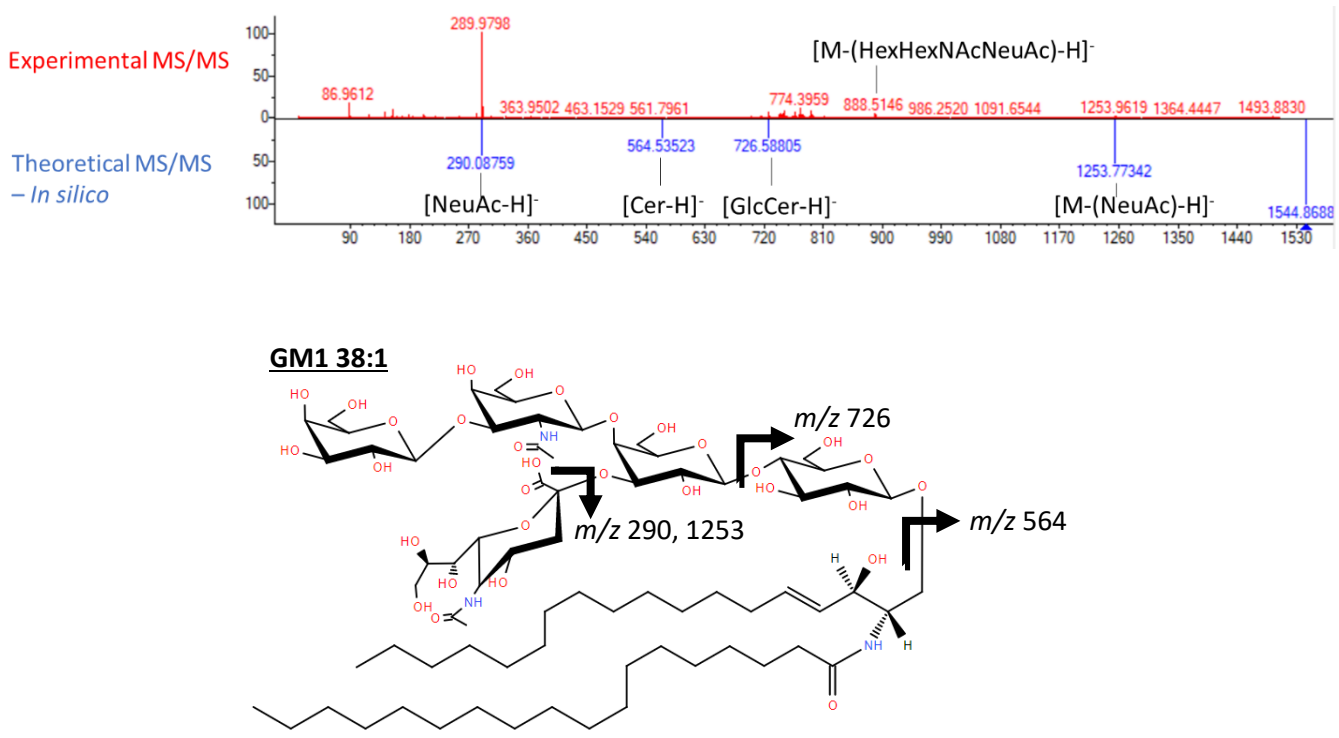

Figure 6. On-tissue negative mode MALDI MSMS characterization of the precursor peak occurring at *m/z* 1544.9. On-tissue MALDI MSMS of the peak at *m/z* 1544.9 produced fragments characteristic of [GM1 38:1-H]$^-$ (d20:0). MSMS product ion spectra visualized using LipidBLAST software[85]. MALDI MSMS was performed at described in Methods. GM1 38:1 molecular structure visualized from LMISSD[93].

3.3 Negative ion MALDI IMS scans detect regional lipid abnormalities within pvWMHs – *m/z* 450-1000 Range

Analysis of negative ion scans conducted at *m/z* 450-1000 revealed differences in expression for 11 of 41 consistently detected ion species (Fig. 7, Table 4). Increased peak intensity was observed for the ions occurring at *m/z* = 932.6, 920.6, 916.6, 878.7, 876.7, 715.6, 644.4, 599.2, 597.2, and 563.3 (Fig. 7). The intensity of the mass peak at *m/z* = 647.0 was found to be significantly decreased in WMHs relative to NAWM (Fig. 7).

Assignment of ion species to significant mass peaks in negative ion low range scans was performed by experimental *m/z* searches in LMISSD and SwissLipids (Table

4). Similarly to the identification of ion species in the higher range negative ion detection mode, on-tissue MALDI MSMS spectra were generated to assist the confident assignment of lipid ion identities. We attempted to generate negative ion MSMS spectra from all significantly altered precursor species, however, the ion species occurring at *m/z* = 878.7, 876.7, 644.4 failed to generate viable MSMS spectra. Similar to product ion spectra generated from high range negative ion precursors, product ion spectra in this range showed fragments at *m/z* = 79, 153, 171 (Table 4). As previously reported, these fragments are characteristic fragments of glycerophospholipids, confirming that all altered lipid ion species in low range negative ion scans are glycerophospholipids (Table 1, 4).

Using this strategy, we assigned tentative lipid ion identities to all mass peaks, except for the mass peak occurring at *m/z* = 647.0 in negative ion low range scans (Table 4).

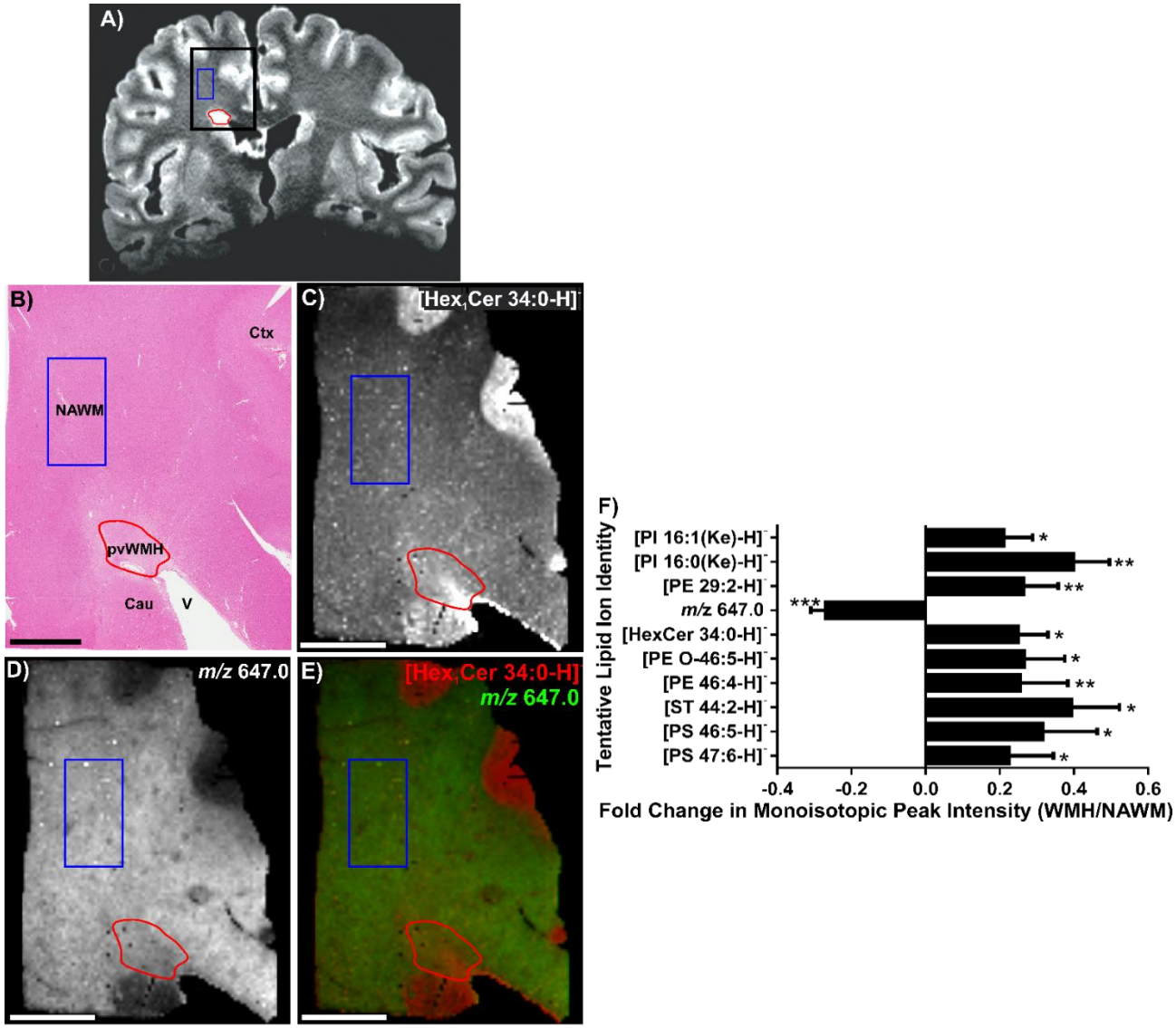

Figure 7. Low range negative ion detection MALDI IMS scans distinguished increased and decreased lipid ion intensity in pvWMHs relative to NAWM in post-mortem human tissue. A) Coronal FLAIR MRI of a post-mortem human brain. Red asterisk indicates region identified as a pvWMH. Black box indicates approximate area that was dissected for sectioning. Red outline indicates extent of pvWMH. Blue outline indicates a region of NAWM. B) H&E. V, Cau, and Ctx indicate ventricle, caudate, and cortex, respectively. Scale bar = 5 mm. C) & D) MALDI IMS scans conducted on post-mortem human brain tissue sublimated with 1,5 DAN matrix. Intensity maps generated from (C) $[Hex_1Cer\ 34:0\text{-}H]^-$ and (D) the mass peak occurring at *m/*z 647.0. Scale bars = 5 mm. E) Pseudocoloured intensity maps showing the overlay of $[Hex_1Cer\ 34:0\text{-}H]^-$ and the mass peak occurring at 647.0 *m/z*. F) pvWMH:NAWM fold-change of monoisotopic peak intensity for statistically significant lipids. Data presented as mean(SD). * indicates $p<0.05$,**$p<0.01$, ***$p<0.001$ via two-tailed Student's T-Test (n=18-20).

Experimental *m/z*	Product Ion *m/z* (MSMS)	Tentative Identification	Theoretical *m/z*	Mass Error (ppm)
932.6431	59.0, 97.0, 119.0, 241.0, 568.4.0, 749.1, 888.9	$[PS\ 47:6-H]^-$	932.6386	4.8357
920.6273	97.0, 119.0, 153.0, 241.0, 283.0, 327.0, 419.2, 522.3, 542.3, 581.2, 727.0, 880.0	$[PS\ 46:5-H]^-$	920.6386	-12.2719
916.6389	59.0, 97.0, 119.0, 124.4, 241.1, 540.4, 871.2	$[ST\ 44:2-H]^-$	916.6548	17.3023
878.6607	N/A	$[PE\ 46:4-H]^-$	878.6644	-4.2462
876.6714	N/A	$[PE\ O-47:5-H]^-$	876.6852	-15.7183
716.5751	79.0, 153.0, 171.0, 226.0, 281.2, 419.3, 505.4	$[Hex_1Cer\ 34:0-H]^-$	716.5682	9.6516
646.9677	N/A	Unidentified	N/A	N/A
644.4351	79.0, 153.0, 171.0, 226.1.0, 281.2, 479.3, 505.4	$[PE\ 29:2-H]^-$	644.4297	8.4307
599.2397	79.0, 140.0, 153.0, 171.0, 255.2, 283.3, 419.4, 535.0	$[PI\ 16:0(Ke)-H]^-$	599.2474	-12.8194
597.2254	79, 97, 153, 255.2, 283.3, 419.3, 535.5	$[PI\ 16:1(Ke)-H]^-$	597.2318	-10.6742
563.2596	79.0, 153.0, 171.0, 226.2, 308.5, 394.4, 489.5	Indistinguishable structural isomers (Oxidized glycerophospholipids)	563.2627	-5.5036

Table 4. Identification of significantly altered lipid ions detected in negative ion low-range scans by database interrogation and negative mode on-tissue MALDI MSMS

in formalin-fixed post-mortem human white matter. Peaks detected in mass spectra generated using a Sciex 5800 TOF/TOF system, from DAN-coated post-mortem human brain tissue in negative ion mode at *m/z* 450 – 1000 *m/z*. Theoretical *m/z* values and tentative IDs based on experimental *m/z* searches in LMISSD, SwissLipids, complemented with manual interrogation of on-tissue MALDI MSMS as described in Methods.

3.4 Regional phosphatidylcholine and sphingomyelin abnormalities detected using positive ion MALDI IMS scans within pvWMHs

Spectra generated at *m/z* 450-1000 in positive ion mode showed significant increases in the four ion species detected at *m/z* = 764.8, 734.7, 725.6, and 703.6 (Fig. 8), with a simultaneous decrease in the six ion species detected at *m/z* = 848.7, 774.7, 772.7, 746.7, 550.4, and 504.4 (Fig. 8).

Identification of previously unidentified positive ion mass peaks was performed by experimental *m/z* searches of the LMISSD and SwissLipids databases (Table 5). On-tissue MALDI MSMS was also conducted in positive ion detection mode (Table 5). Using this approach, we identified all significantly different mass peaks detected in positive mode scans, except for the mass peaks detected at *m/z* = 764.8 and 734.7 (Fig. 8, Table 5).

Manual interrogation of positive ion product spectra generated using on-tissue MALDI MSMS revealed the presence of a characteristic PC and SM headgroup fragment[98], *m/z* 184 = $[\text{phosphocholine+H}]^+$, in all product spectra (Table 5). The presence of this headgroup fragment in all product spectra generated from species detected in positive mode confirms that positive mode MALDI IMS scans of white matter tissue abundantly detects PC and SM species[99]. Due to the presence of a product ion fragment at *m/z* 184, database searches in LMISSD and SwissLipids for species detected in positive mode scans were limited to lipid species which contain a phosphocholine in

their headgroup, an approach which dramatically reduced the number of potential identities.

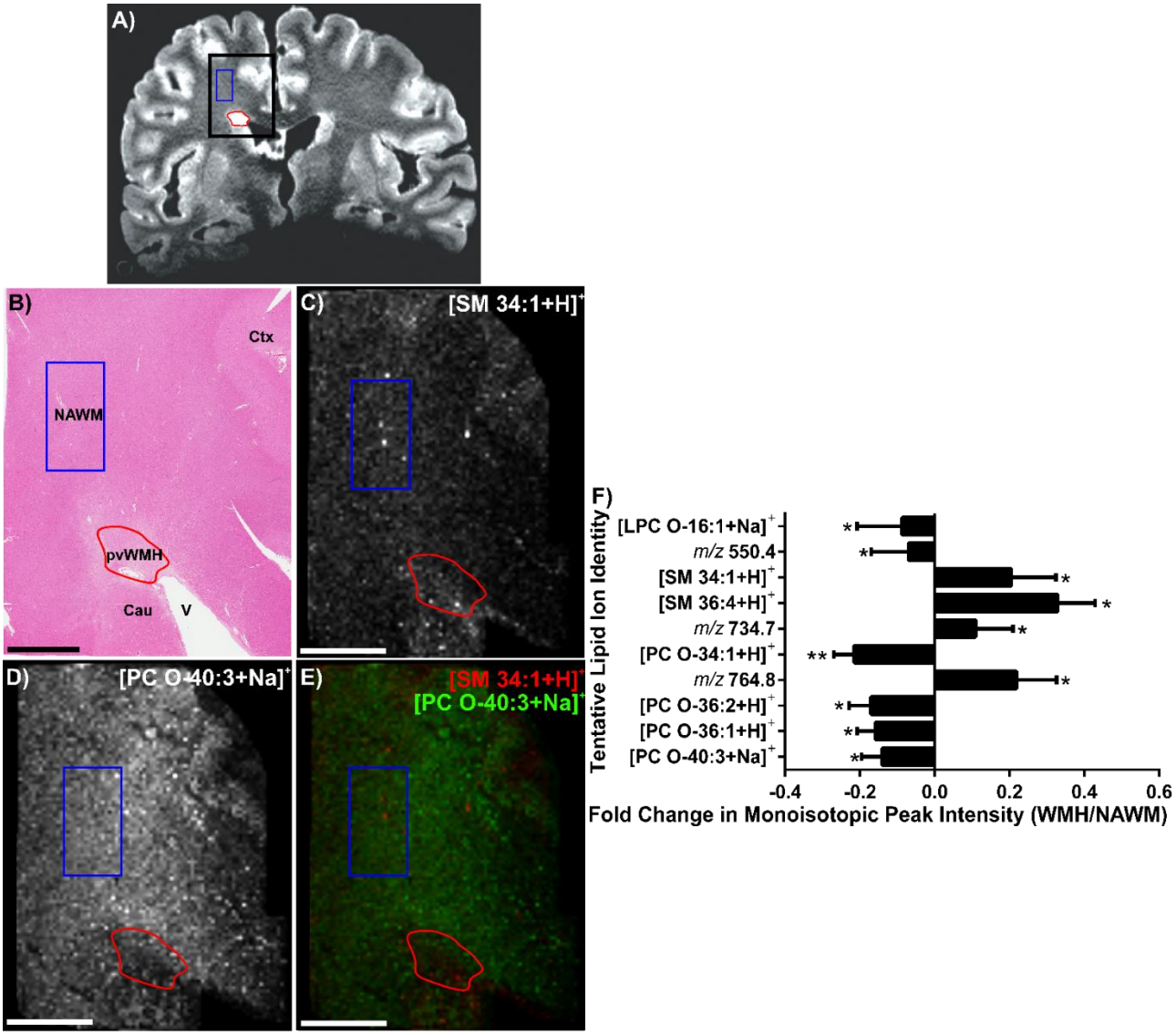

Figure 8. Low range positive ion detection MALDI IMS scans distinguished increased and decreased lipid ion intensity in pvWMHs relative to NAWM in post-mortem human tissue. A) Coronal FLAIR MRI of a post-mortem human brain. Red asterisk indicates region identified as a pvWMH. Black box indicates approximate area that was dissected for sectioning. Red outline indicates extent of pvWMH. Blue outline indicates a region of NAWM. B) H&E. V, Cau, and Ctx indicate ventricle, caudate, and cortex, respectively. Scale bar = 5 mm. C) & D) MALDI IMS scans conducted on post-mortem human brain tissue sublimated with 2,5 DHB matrix. Intensity maps generated from the mass peak occurring at (C) $[SM\ 34:1+H]^+$. and (D) $[PC\ O\text{-}34:3+Na]^+$. Scale bars = 5 mm. E) Pseudocoloured intensity maps showing the overlay of $[SM\ 34:1+H]^+$ and PC $O\text{-}34:3+Na]^+$. E) pvWMH:NAWM fold-change of monoisotopic peak intensity for

statistically significant lipids. Data presented as mean(SD) * indicates p<0.05,**p<0.01 via two-tailed Student's T-Test (n=16-20).

Experimental *m/z*	Product Ion *m/z* (MSMS)	Tentative Identification	Theoretical *m/z*	Mass Error (ppm)
848.7224	39.0, 86.1, 104.1, 163.0, 184.1, 224.0, 454.3, 480.2, 542.6, 659.4, 705.8, 763.9, 792.8, 793.7	[PC O-40:3+Na]$^+$	848.6504	84.8524
774.6687	39.0, 86.1,184.1, 198.1, 390.2, 512.3, 713.9	[PC O-36:1+H]$^+$	774.6372	40.6642
772.6563	39, 86.1,184.1, 198.1, 392.3, 628.6, 711.5	[PC O-36:2+H]$^+$	772.6215	45.0416
764.7509	184.0, 369.3, 410.9, 468.9, 561.2, 632.6, 697.1, 710.5	Unidentified	N/A	N/A
746.6560	86, 184.1, 389.4, 482.3, 683.4	[PC O-34:1+H]$^+$	746.6058	67.2376
734.7445	184.0, 341.4, 419.3, 537.4, 579.4, 608.9, 639.3, 648.5	Unidentified	N/A	N/A
725.6122	37.8, 169.1, 184.0, 307.2, 400.2, 430.8, 567.1, 670.4	[SM 36:4+H]$^+$	725.5592	73.047106
703.6105	171.1, 184.1, 425.2, 520.2, 525.5, 599.3, 634.4, 652.4	[SM 34:1+H]$^+$	703.5749	50.5987
550.4082	184.1, 264.3, 401.4, 487.5, 503.7	Indistinguishable [PC or LPC+H H]$^+$	550.3867	39.0634
504.3605	60.0, 104.1, 184.0, 342.8, 382.2, 436.3, 446.1	[LPC O-16:0+Na]$^+$	504.3424	35.8883

Table 5. Identification of significantly altered lipid ions detected in positive ion low-range scans by database interrogation and positive mode on-tissue MALDI MSMS in formalin-fixed post-mortem human white matter. Peaks detected in mass spectra generated using a Sciex 5800 TOF/TOF system, from DHB-coated post-mortem human brain tissue in positive ion mode at *m/z* 450 – 1000 *m/z*. Theoretical *m/z* values and

tentative IDs based on experimental *m/z* searches in LMISSD, SwissLipids and manual interrogation of on-tissue MALDI MSMS product ion spectra.

CHAPTER 4: DISCUSSION

In this study, we demonstrate for the first time the use of MALDI IMS to identify lipid abnormalities of MRI-defined pvWMHs within formalin-fixed, human brain tissue. As previously shown, MALDI of DAN or DHB-coated tissue was effective for the respective negative or positive ionization of lipids[92]. MALDI IMS scans conducted in negative mode *m/z* 450 – 2000 and positive mode *m/z* 450-1000 permitted the consistent detection (>80% of the 21 tissue blocks) of 116 unique ion species across the three scan modes. Analysis of consistently detected mass peaks elucidated intrasubject differences in lipid expression between NAWM and pvWMHs for 31 lipid ion species. Lipid profile alterations were bi-directional, representing increases in 16 mass peaks and decreases in 15 mass peaks in pvWMHs relative to NAWM. Experimental *m/z* searches in lipid databases, LMISSD and SwissLipids, and manual interrogation of MALDI MSMS product ion spectra, permitted the assignment of lipid ion identities to 27 of the 31 significantly altered mass peaks. This investigation has exhibited the novel use of MALDI IMS for comparative lipid profile characterization of healthy and pathological tissue in clinically relevant, formalin-fixed, human brain tissue.

The consistent detection of 116 mass peaks amongst all tissue samples corresponding to positive and negative ions at *m/z* 450 – 2000 demonstrates the potential of MALDI IMS for broad, untagged approach to lipid investigations. Although these consistently detected species do not represent the totality of lipids that are present in human white matter, as some lipid species may not ionize in the presence of either DAN or DHB matrix, it does represent a broad profile of the lipid species present in human

white matter. This application is better suited for a ‘rule-in’ rather than ‘rule-out’ approach due to the aforementioned poor ionization of certain lipid species, or ion suppression from readily-ionized molecules such as PC species in positive ion mode[99]. This ‘rule-in’ approach is important to consider when assessing lipid abnormalities in formalin-fixed tissue as formalin is known to degrade the signal of phosphoethanolamines, thus making phosphoethanolamine abnormalities less apparent[100].

Gangliosides are ubiquitously expressed lipids that are highly enriched in neural tissue[101]. Gangliosides are an integral membrane component of many cell populations within the CNS, where they play critical roles in the structure of the plasma membrane, as well as influencing the localization of proteins within the plasma membrane[102]. Ganglioside abnormalities have previously been associated with neurodegenerative diseases such as Alzheimer’s disease, stroke, and multiple sclerosis[102,103]. Interestingly, we observed an increase in the intensity of mass peaks associated with negative ions of GM1 36:1 (18:0) and GM1 38:1 (d20:0) in pvWMHs relative to NAWM. The GM1 ganglioside species have previously been associated with neuroprotective effects[102]. Numerous mechanisms for the neuroprotective effects of GM1 species have been proposed, including the inhibition nitric oxide synthase activity[104], prevention of glutamate toxicity[105], and influencing the activity of protein receptors via membrane microdomain organization[106]. Therefore the effects of GM1 species in pvWMHs are likely multimodal, varying depending on the cell population in-question[102]. Thus, further work is required to elucidate what cell population, or populations, are responsible for the observed increase of GM1 in pvWMHs.

An interesting observation in the imaging data is that some lipid species elevated in the pvWMH were also elevated in the adjacent caudate. Our current understanding of this observation is limited, however, a proposed cause of this may be leakage of biological macromolecules from vicinal regions into the pvWMH during the development of the pvWMH. Factors such as localized tissue rarefaction and edema in the pvWMH may play a role in the leakage of molecules from vicinal regions, and vice-versa[13,22]. PvWMHs are known to be progressive, however, molecular mechanisms behind the spreading pathology of pvWMHs remain somewhat limited[107]. Whilst speculative, if this leakage phenomenon were confirmed, this could suggest a potential molecular mechanism for the propagation of pvWMHs into adjacent regions.

Confident assignment of lipid ion identity is a critical aspect of any investigation of lipid abnormalities. In the current study, assignment of lipid identity was attempted by searching experimental *m/z* values in two independent databases, LipidMAPS and SwissLipids, and assisted by manual interrogation of product ion spectra generated by on-tissue MALDI MSMS. A limitation currently facing the use of MALDI IMS for analysis of formalin-fixed tissue is the difficulty in assigning ion species identities to mass peaks using MS^n. MS^1 is unable distinguishing structural isomers, thus demonstrating the need for MSMS-based identification. Manual interrogation of MSMS spectra for the presence of characteristic peaks has previously been used to assist lipid identity assignment[87]. However, this technique is not feasible for complete structural characterization of all significantly altered species identified in pvWMHs in the current study. Other publications in the field of lipid analysis have noted that the popular use of MALDI mass spectrometry as a tool for protein analysis has contributed to the development of software for the

identification of proteins, however, software for lipid identification is notably trailing[108,109]. We believe future studies using MALDI IMS for lipid detection would benefit from the development of species-specific and tissue-specific lipid identification databases.

Conclusions

In conclusion, we have demonstrated the viability of using MALDI IMS for a broad, untagged approach to lipid detection in archived, formalin-fixed, post-mortem human brain tissue. This approach permitted the consistent detection of 116 distinct ion species in 21 tissue blocks from 11 brains. We have shown the application of MALDI IMS for resolving intrasubject differences in lipid expression by detecting bidirectional differences in mass peak intensity between pvWMHs and adjacent NAWM. By interrogating two independent lipid databases, LipidMAPS and SwissLipids, as well as conducting on-tissue MALDI MSMS, we assigned tentative lipid ions identities to 27 mass peaks. Interestingly, two observed differences were increases of the neuroprotective gangliosides GM1 36:1 (d18:0) and GM1 38:1 (d20:0) in pvWMHs relative to NAWM. Further investigation is required to identify what cell population is responsible for the observed elevation in GM1 species and the biological ramifications of elevated GM1 in WMHs. Assignment of lipid ion identities to the remaining mass peaks represents a limitation of lipid analysis in formalin-fixed non-embedded post-mortem human tissue, however, we believe that advancements in lipid-related software will continue to contribute to high-throughput bioinformatic-scale lipid analysis using MALDI IMS. In summary, this study demonstrates the potential of MALDI IMS for the purpose of spatial-specific lipid quantification in MRI-defined, formalin-fixed, post-mortem human tissue and identifies lipid alterations associated with pvWMHs.

REFERENCES

(1) Prince, A. M.; Wimo, A.; Guerchet, M.; Ali, M. G.-C.; Wu, Y.-T.; Prina, M.; Chan, K. Y.; Xia, Z. World Alzheimer Report 2015 The Global Impact of Dementia An AnAlysIs of PrevAlence, IncIDence, CosT AnD TrenDs.

(2) Brookmeyer, R.; Johnson, E.; Ziegler-Graham, K.; Arrighi, H. M. Forecasting the Global Burden of Alzheimer's Disease. *Alzheimer's Dement.* **2007**, *3* (3), 186–191. https://doi.org/10.1016/J.JALZ.2007.04.381.

(3) Dementia Statistics | Alzheimer's Disease International (ADI).

(4) Miller, K. L.; Stagg, C. J.; Douaud, G.; Jbabdi, S.; Smith, S. M.; Behrens, T. E. J.; Jenkinson, M.; Chance, S. A.; Esiri, M. M.; Voets, N. L.; Jenkinson, N.; Aziz, T. Z.; Turner, M. R.; Johansen-Berg, H.; McNab, J. A. Diffusion Imaging of Whole, Post-Mortem Human Brains on a Clinical MRI Scanner. *Neuroimage* **2011**, *57* (1), 167–181. https://doi.org/10.1016/J.NEUROIMAGE.2011.03.070.

(5) González, R. G. Clinical MRI of Acute Ischemic Stroke. *J. Magn. Reson. Imaging* **2012**, *36* (2), 259–271. https://doi.org/10.1002/JMRI.23595.

(6) Bangerter, N. K.; Hargreaves, B. A.; Gold, G. E.; Stucker, D. T.; Nishimura, D. G. Fluid-Attenuated Inversion-Recovery SSFP Imaging. *J. Magn. Reson. Imaging* **2006**, *24* (6), 1426–1431. https://doi.org/10.1002/JMRI.20743/FULL.

(7) MA, T.; FW, F.; D, K.; ET, H.; KS, K.; PM, T.; MN, B. White Matter Hyperintensities and Their Relationship to Cognition: Effects of Segmentation Algorithm. *Neuroimage* **2020**, *206*. https://doi.org/10.1016/J.NEUROIMAGE.2019.116327.

(8) Lazarus, R.; Prettyman, R.; Cherryman, G. White Matter Lesions on Magnetic Resonance Imaging and Their Relationship with Vascular Risk Factors in Memory Clinic Attenders. *Int. J. Geriatr. PSYCHIATRY Int J Geriatr Psychiatry* **2005**, *20*, 274–279. https://doi.org/10.1002/gps.1283.

(9) Prins, N. D.; Scheltens, P. White Matter Hyperintensities, Cognitive Impairment and Dementia: An Update. *Nat. Rev. Neurol. 2015 113* **2015**, *11* (3), 157–165. https://doi.org/10.1038/nrneurol.2015.10.

(10) Debette, S.; Markus, H. S. The Clinical Importance of White Matter Hyperintensities on Brain Magnetic Resonance Imaging: Systematic Review and Meta-Analysis. *BMJ (Online)*. 2010, p 288. https://doi.org/10.1136/bmj.c3666.

(11) H, B.; C, B.; A, P.; L, P.; D, I.; H, C.; T, E.; F, F.; JM, F.; P, L.; J, O.; P, S.; MC, V.; LO, W.; G, W.; A, W.; MG, H. Association of Gait and Balance Disorders with Age-Related White Matter Changes: The LADIS Study. *Neurology* **2008**, *70* (12), 935–942. https://doi.org/10.1212/01.WNL.0000305959.46197.E6.

(12) Wardlaw, J. M.; Hernández, M. C. V.; Muñoz-Maniega, S. What Are White Matter Hyperintensities Made of?: Relevance to Vascular Cognitive Impairment. *J. Am. Hear. Assoc. Cardiovasc. Cerebrovasc. Dis.* **2015**, *4* (6), 1140. https://doi.org/10.1161/JAHA.114.001140.

(13) Fazekas, F.; Kleinert, R.; Offenbacher, H.; Payer, F.; Schmidt, R.; Kleinert, G.; Radner, H.; Lechner, H. The Morphologic Correlate of Incidental Punctate White Matter Hyperintensities on MR Images. *Am. J. Roentgenol.* **1991**, *157* (6), 1317–1323.

(14) Yoshita, M.; Fletcher, E.; Harvey, D.; Ortega, M.; Martinez, O.; Mungas, D. M.; Reed, B. R.; DeCarli, C. S. Extent and Distribution of White Matter Hyperintensities in Normal Aging, MCI, and AD. *Neurology* **2006**, *67* (12), 2192. https://doi.org/10.1212/01.WNL.0000249119.95747.1F.

(15) Love, S.; Miners, J. S. White Matter Hypoperfusion and Damage in Dementia: Post-Mortem Assessment. *Brain Pathol.* **2015**, *25* (1), 99–107. https://doi.org/10.1111/BPA.12223.

(16) Fernando, M. S.; Simpson, J. E.; Matthews, F.; Brayne, C.; Lewis, C. E.; Barber, R.; Kalaria, R. N.; Forster, G.; Esteves, F.; Wharton, S. B.; Shaw, P. J.; O'Brien, J. T.; Ince, P. G. White Matter Lesions in an Unselected Cohort of the Elderly. *Stroke* **2006**, *37* (6), 1391–1398. https://doi.org/10.1161/01.STR.0000221308.94473.14.

(17) Roseborough, A.; Langdon, K.; Hammond, R.; Pasternak, S.; Khan, A.; Whitehead, S. Microvessel Stenosis and Density Analysis of Post Mortem WMH Detected Using Ultra High Field MRI in Aging, Cerebrovascular and Alzheimer Disease. *FASEB J.* **2019**, *33* (S1), 496.47-496.47. https://doi.org/10.1096/FASEBJ.2019.33.1_SUPPLEMENT.496.47.

(18) M, D.; R, R.; E, C.; E, J.; D, H.; H, C.; M, D. Incident Subcortical Infarcts Induce Focal Thinning in Connected Cortical Regions. *Neurology* **2012**, *79* (20), 2025–2028. https://doi.org/10.1212/WNL.0B013E3182749F39.

(19) R, S.; C, E.; S, R.; H, S.; F, F. Progression of Cerebral White Matter Lesions: 6-Year Results of the Austrian Stroke Prevention Study. *Lancet (London, England)*

2003, *361* (9374), 2046–2048. https://doi.org/10.1016/S0140-6736(03)13616-1.

(20) MS, F.; JT, O.; RH, P.; P, E.; G, F.; W, M.; JY, S.; A, G.; FE, M.; R, B.; RN, K.; PG, I. Comparison of the Pathology of Cerebral White Matter with Post-Mortem Magnetic Resonance Imaging (MRI) in the Elderly Brain. *Neuropathol. Appl. Neurobiol.* **2004**, *30* (4), 385–395. https://doi.org/10.1111/J.1365-2990.2004.00550.X.

(21) R, S.; H, S.; J, H.; M, L.; S, W.; M, C.; S, S.; C, E.; S, R.; T, E.; L, P.; P, S.; F, F.; K, J. Heterogeneity in Age-Related White Matter Changes. *Acta Neuropathol.* **2011**, *122* (2), 171–185. https://doi.org/10.1007/S00401-011-0851-X.

(22) Fazekas, F.; Kleinert, R.; Offenbacher, H.; Schmidt, R.; Kleinert, G.; Payer, F.; Radner, H.; Lechner, H. Pathologic Correlates of Incidental Mri White Matter Signal Hyperintensities. *Neurology* **1993**, *43* (9), 1683–1689. https://doi.org/10.1212/wnl.43.9.1683.

(23) Janmey, P. A.; Kinnunen, P. K. J. Biophysical Properties of Lipids and Dynamic Membranes. *Trends in Cell Biology*. 2006. https://doi.org/10.1016/j.tcb.2006.08.009.

(24) Harayama, T.; Riezman, H. Understanding the Diversity of Membrane Lipid Composition. *Nat. Rev. Mol. Cell Biol. 2018 195* **2018**, *19* (5), 281–296. https://doi.org/10.1038/nrm.2017.138.

(25) Cullis, P. R.; Fenske, D. B.; Hope, M. J. *Physical Properties and Functional Roles of Lipids in Membranes*; Vance, D. E., Vance, J. E., Eds.; Elsevier, 1996.

(26) Hashidate-Yoshida, T.; Harayama, T.; Hishikawa, D.; Morimoto, R.; Hamano, F.; Tokuoka, S. M.; Eto, M.; Tamura-Nakano, M.; Yanobu-Takanashi, R.; Mukumoto, Y.; Kiyonari, H.; Okamura, T.; Kita, Y.; Shindou, H.; Shimizu, T. Fatty Acid Remodeling by LPCAT3 Enriches Arachidonate in Phospholipid Membranes and Regulates Triglyceride Transport. *Elife* **2015**, *4*. https://doi.org/10.7554/ELIFE.06328.

(27) M, P.; S, V.; S, P.; S, L.-G.; LA, P.; T, F.; R, G.; B, G.; B, A.; H, B. Lipid Cell Biology. Polyunsaturated Phospholipids Facilitate Membrane Deformation and Fission by Endocytic Proteins. *Science* **2014**, *345* (6197), 693–697. https://doi.org/10.1126/SCIENCE.1255288.

(28) FX, C.; AM, E.; P, H.; P, B.; E, L.; B, G.; C, T.; A, E.; von Heijne G; C, T.; R, P.; F, W.; B, B. Molecular Recognition of a Single Sphingolipid Species by a Protein's Transmembrane Domain. *Nature* **2012**, *481* (7382), 525–529. https://doi.org/10.1038/NATURE10742.

(29) E, S.; I, L.; S, M.; C, E. The Mystery of Membrane Organization: Composition, Regulation and Roles of Lipid Rafts. *Nat. Rev. Mol. Cell Biol.* **2017**, *18* (6), 361–374. https://doi.org/10.1038/NRM.2017.16.

(30) Zemski Berry, K. A.; Hankin, J. A.; Barkley, R. M.; Spraggins, J. M.; Caprioli, R. M.; Murphy, R. C. MALDI Imaging of Lipid Biochemistry in Tissues by Mass Spectrometry. *Chemical Reviews*. 2011, pp 6491–6512. https://doi.org/10.1021/cr200280p.

(31) Kraft, M. L. Plasma Membrane Organization and Function: Moving Past Lipid

Rafts. *Mol. Biol. Cell* **2013**, *24* (18), 2765. https://doi.org/10.1091/MBC.E13-03-0165.

(32) D, B.; M, P.; N, C.; I, R.; H, R.; A, R.; TC, W.; R, L. Plasma Membrane Stress Induces Relocalization of Slm Proteins and Activation of TORC2 to Promote Sphingolipid Synthesis. *Nat. Cell Biol.* **2012**, *14* (5), 542–547. https://doi.org/10.1038/NCB2480.

(33) Maxfield, F. R. Plasma Membrane Microdomains. *Curr. Opin. Cell Biol.* **2002**, *14* (4), 483–487. https://doi.org/10.1016/S0955-0674(02)00351-4.

(34) LJ, P. Rafts Defined: A Report on the Keystone Symposium on Lipid Rafts and Cell Function. *J. Lipid Res.* **2006**, *47* (7), 1597–1598. https://doi.org/10.1194/JLR.E600002-JLR200.

(35) JF, H. Lipid Rafts: Contentious Only from Simplistic Standpoints. *Nat. Rev. Mol. Cell Biol.* **2006**, *7* (6), 456–462. https://doi.org/10.1038/NRM1925.

(36) S, P.; G, M.; LR, Y.; ML, G. NGF Causes TrkA to Specifically Attract Microtubules to Lipid Rafts. *PLoS One* **2012**, *7* (4). https://doi.org/10.1371/JOURNAL.PONE.0035163.

(37) Casares, D.; Escribá, P. V; Rosselló, C. A. Membrane Lipid Composition: Effect on Membrane and Organelle Structure, Function and Compartmentalization and Therapeutic Avenues. *Int. J. Mol. Sci.* **2019**, *20* (9). https://doi.org/10.3390/IJMS20092167.

(38) Sprong, H.; van der Sluijs, P.; van Meer, G. How Proteins Move Lipids and Lipids

Move Proteins. *Nat. Rev. Mol. Cell Biol. 2001 27* **2001**, *2* (7), 504–513. https://doi.org/10.1038/35080071.

(39) Jensen, M.; Mouritsen, O. G. Lipids Do Influence Protein Function—the Hydrophobic Matching Hypothesis Revisited. *Biochim. Biophys. Acta - Biomembr.* **2004**, *1666* (1–2), 205–226. https://doi.org/10.1016/J.BBAMEM.2004.06.009.

(40) Grau-Campistany, A.; Strandberg, E.; Wadhwani, P.; Reichert, J.; Bürck, J.; Rabanal, F.; Ulrich, A. S. Hydrophobic Mismatch Demonstrated for Membranolytic Peptides and Their Use as Molecular Rulers to Measure Bilayer Thickness in Native Cells. *Sci. Reports 2015 51* **2015**, *5* (1), 1–9. https://doi.org/10.1038/srep09388.

(41) Kabbani, A. M.; Raghunathan, K.; Lencer, W. I.; Kenworthy, A. K.; Kelly, C. V. Structured Clustering of the Glycosphingolipid GM1 Is Required for Membrane Curvature Induced by Cholera Toxin. *Proc. Natl. Acad. Sci.* **2020**, *117* (26), 14978–14986. https://doi.org/10.1073/PNAS.2001119117.

(42) Ernst, R.; Ejsing, C. S.; Antonny, B. Homeoviscous Adaptation and the Regulation of Membrane Lipids. *J. Mol. Biol.* **2016**, *428* (24), 4776–4791. https://doi.org/10.1016/J.JMB.2016.08.013.

(43) Pagliuso, A.; Valente, C.; Giordano, L. L.; Filograna, A.; Li, G.; Circolo, D.; Turacchio, G.; Marzullo, V. M.; Mandrich, L.; Zhukovsky, M. A.; Formiggini, F.; Polishchuk, R. S.; Corda, D.; Luini, A. Golgi Membrane Fission Requires the CtBP1-S/BARS-Induced Activation of Lysophosphatidic Acid Acyltransferase δ. *Nat. Commun.* **2016**, *7*. https://doi.org/10.1038/NCOMMS12148.

(44) Rusten, T. E.; Stenmark, H. Analyzing Phosphoinositides and Their Interacting Proteins. *Nat. Methods 2006 34* **2006**, *3* (4), 251–258. https://doi.org/10.1038/nmeth867.

(45) K, M. IP3 Receptor/Ca2+ Channel: From Discovery to New Signaling Concepts. *J. Neurochem.* **2007**, *102* (5), 1426–1446. https://doi.org/10.1111/J.1471-4159.2007.04825.X.

(46) Y, N. Intracellular Signaling by Hydrolysis of Phospholipids and Activation of Protein Kinase C. *Science* **1992**, *258* (5082), 607–614. https://doi.org/10.1126/SCIENCE.1411571.

(47) Y, A.; S, N.; K, Y.; Y, N. Protein Kinase C, Calcium and Phospholipid Degradation. *Trends Biochem. Sci.* **1992**, *17* (10), 414–417. https://doi.org/10.1016/0968-0004(92)90011-W.

(48) Berridge, M. J. The Inositol Trisphosphate/Calcium Signaling Pathway in Health and Disease. *https://doi.org/10.1152/physrev.00006.2016* **2016**, *96* (4), 1261–1296. https://doi.org/10.1152/PHYSREV.00006.2016.

(49) GE, S. Calcium Dysregulation, IP3 Signaling, and Alzheimer's Disease. *Neuroscientist* **2005**, *11* (2), 110–115. https://doi.org/10.1177/1073858404270899.

(50) Demuro, A.; Parker, I. Cytotoxicity of Intracellular Aβ42 Amyloid Oligomers Involves Ca2+ Release from the Endoplasmic Reticulum by Stimulated Production of Inositol Trisphosphate. *J. Neurosci.* **2013**, *33* (9), 3824. https://doi.org/10.1523/JNEUROSCI.4367-12.2013.

(51) SB, M.; PT, I.; D, D.; RC, H.; HA, B. A Targeted Mass Spectrometric Analysis of Phosphatidylinositol Phosphate Species. *J. Lipid Res.* **2005**, *46* (8), 1796–1802. https://doi.org/10.1194/JLR.D500010-JLR200.

(52) Kim, Y.; Shanta, S. R.; Zhou, L.-H.; Kim, K. P. Mass Spectrometry Based Cellular Phosphoinositides Profiling and Phospholipid Analysis: A Brief Review. *Exp. Mol. Med.* **2010**, *42* (1), 1–11. https://doi.org/10.3858/emm.2010.42.1.001.

(53) T, M.; A, T.; T, M.; M, H.; N, F. Ganglioside GM1 Binds to the Trk Protein and Regulates Receptor Function. *Proc. Natl. Acad. Sci. U. S. A.* **1995**, *92* (11), 5087–5091. https://doi.org/10.1073/PNAS.92.11.5087.

(54) Ferrari, G.; Greene, L. A. Prevention of Apoptotic Neuronal Death by G(M1) Ganglioside. Involvement of Trk Neurotrophin Receptors. *J. Biol. Chem.* **1995**, *270* (7), 3074–3080. https://doi.org/10.1074/JBC.270.7.3074.

(55) RW, L.; G, W. The Multi-Tasked Life of GM1 Ganglioside, a True Factotum of Nature. *Trends Biochem. Sci.* **2015**, *40* (7), 407–418. https://doi.org/10.1016/J.TIBS.2015.04.005.

(56) E, C.; ED, B.; M, M.; G, L.; M, F.; DY, P.; R, C.; N, L.; L, M.; S, S. GM1 Promotes TrkA-Mediated Neuroblastoma Cell Differentiation by Occupying a Plasma Membrane Domain Different from TrkA. *J. Neurochem.* **2019**, *149* (2), 231–241. https://doi.org/10.1111/JNC.14685.

(57) Caughlin, S.; Park, D. H.; Yeung, K. K. C.; Cechetto, D. F.; Whitehead, S. N. Sublimation of DAN Matrix for the Detection and Visualization of Gangliosides in Rat Brain Tissue for MALDI Imaging Mass Spectrometry. *J. Vis. Exp.* **2017**, *2017*

(121). https://doi.org/10.3791/55254.

(58) Harris, A.; Roseborough, A.; Mor, R.; Yeung, K. K. C.; Whitehead, S. N. Ganglioside Detection from Formalin-Fixed Human Brain Tissue Utilizing MALDI Imaging Mass Spectrometry. *J. Am. Soc. Mass Spectrom.* **2020**, *31* (3), 479–487. https://doi.org/10.1021/jasms.9b00110.

(59) Adibhatla, R. M.; Hatcher, J. F. Role of Lipids in Brain Injury and Diseases. *Future Lipidology*. 2007, pp 403–422. https://doi.org/10.2217/17460875.2.4.403.

(60) Mulder, I. A.; Ogrinc Potočnik, N.; Broos, L. A. M.; Prop, A.; Wermer, M. J. H.; Heeren, R. M. A.; van den Maagdenberg, A. M. J. M. Distinguishing Core from Penumbra by Lipid Profiles Using Mass Spectrometry Imaging in a Transgenic Mouse Model of Ischemic Stroke. *Sci. Rep.* **2019**, *9* (1). https://doi.org/10.1038/s41598-018-37612-5.

(61) Wong, M. W.; Braidy, N.; Poljak, A.; Pickford, R.; Thambisetty, M.; Sachdev, P. S. Dysregulation of Lipids in Alzheimer's Disease and Their Role as Potential Biomarkers. *Alzheimer's and Dementia*. 2017, pp 810–827. https://doi.org/10.1016/j.jalz.2017.01.008.

(62) Lee, J.; Kosaras, B.; Signore, S. J. Del; Cormier, K.; McKee, A.; Ratan, R. R.; Kowall, N. W.; Ryu, H. Modulation of Lipid Peroxidation and Mitochondrial Function Improves Neuropathology in Huntington's Disease Mice. *Acta Neuropathol. 2010 1214* **2010**, *121* (4), 487–498. https://doi.org/10.1007/S00401-010-0788-5.

(63) Dong, Y.; D'Mello, C.; Pinsky, W.; Lozinski, B. M.; Kaushik, D. K.; Ghorbani, S.;

Moezzi, D.; Brown, D.; Melo, F. C.; Zandee, S.; Vo, T.; Prat, A.; Whitehead, S. N.; Yong, V. W. Oxidized Phosphatidylcholines Found in Multiple Sclerosis Lesions Mediate Neurodegeneration and Are Neutralized by Microglia. *Nat. Neurosci. 2021 244* **2021**, *24* (4), 489–503. https://doi.org/10.1038/s41593-021-00801-z.

(64) Dawson, G. Measuring Brain Lipids. *Biochim. Biophys. Acta* **2015**, *1851* (8), 1026. https://doi.org/10.1016/J.BBALIP.2015.02.007.

(65) Baker, T. C.; Han, J.; Borchers, C. H. Recent Advancements in Matrix-Assisted Laser Desorption/Ionization Mass Spectrometry Imaging. *Curr. Opin. Biotechnol.* **2017**, *43*, 62–69. https://doi.org/10.1016/J.COPBIO.2016.09.003.

(66) Murphy, R. C.; Hankin, J. A.; Barkley, R. M. Imaging of Lipid Species by MALDI Mass Spectrometry. *J. Lipid Res.* **2009**, *50* (SUPPL.), S317–S322. https://doi.org/10.1194/JLR.R800051-JLR200.

(67) Watson, J. T.; Sparkman, O. D. *Introduction to Mass Spectrometry: Instrumentation, Applications, and ... - J. Throck Watson, O. David Sparkman - Google Books*, 4th ed.; John Wiley & Sons, 2007.

(68) Stoeckli, M.; Chaurand, P.; Hallahan, D. E.; Caprioli, R. M. Imaging Mass Spectrometry: A New Technology for the Analysis of Protein Expression in Mammalian Tissues. *Nat. Med. 2001 74* **2001**, *7* (4), 493–496. https://doi.org/10.1038/86573.

(69) Kind, T.; Fiehn, O. Advances in Structure Elucidation of Small Molecules Using Mass Spectrometry. *Bioanal. Rev. 2010 21* **2010**, *2* (1), 23–60. https://doi.org/10.1007/S12566-010-0015-9.

(70) Lai, Y.-H.; Wang, Y.-S. Matrix-Assisted Laser Desorption/Ionization Mass Spectrometry: Mechanistic Studies and Methods for Improving the Structural Identification of Carbohydrates. *Mass Spectrom.* **2017**, *6* (Spec Iss 2), S0072–S0072. https://doi.org/10.5702/MASSSPECTROMETRY.S0072.

(71) Petković, M.; Schiller, J.; Müller, M.; Benard, S.; Reichl, S.; Arnold, K.; Arnhold, J. Detection of Individual Phospholipids in Lipid Mixtures by Matrix-Assisted Laser Desorption/Ionization Time-of-Flight Mass Spectrometry: Phosphatidylcholine Prevents the Detection of Further Species. *Anal. Biochem.* **2001**, *289* (2), 202–216. https://doi.org/10.1006/ABIO.2000.4926.

(72) Murphy, R. C.; Hankin, J. A.; Barkley, R. M. Imaging of Lipid Species by MALDI Mass Spectrometry. *J. Lipid Res.* **2009**, *50* (Suppl), S317. https://doi.org/10.1194/JLR.R800051-JLR200.

(73) Fenn, J. B.; Mann, M.; Meng, C. K.; Wong, S. F.; Whitehouse, C. M. Electrospray Ionization for Mass Spectrometry of Large Biomolecules. *Science (80-.).* **1989**, *246* (4926), 64–71. https://doi.org/10.1126/SCIENCE.2675315.

(74) A, N.; A, P.; M, S. Limitations of Electrospray Ionization in the Analysis of a Heterogeneous Mixture of Naturally Occurring Hydrophilic and Hydrophobic Compounds. *Rapid Commun. Mass Spectrom.* **2010**, *24* (21), 3163–3170. https://doi.org/10.1002/RCM.4749.

(75) Ho, C. S.; Lam, C. W. K.; Chan, M. H. M.; Cheung, R. C. K.; Law, L. K.; Lit, L. C. W.; Ng, K. F.; Suen, M. W. M.; Tai, H. L. Electrospray Ionisation Mass Spectrometry: Principles and Clinical Applications. *Clin. Biochem. Rev.* **2003**, *24*

(1), 3.

(76) P, K.; UH, V. Electrospray: From Ions in Solution to Ions in the Gas Phase, What We Know Now. *Mass Spectrom. Rev.* **2009**, *28* (6), 898–917. https://doi.org/10.1002/MAS.20247.

(77) KA, A.-S.; V, Z.; WF, S.; NR, K.; RM, H.; HH, H. Matrix-Assisted Laser Desorption/Ionization Time-of-Flight Mass Spectrometry of Lipids: Ionization and Prompt Fragmentation Patterns. *Rapid Commun. Mass Spectrom.* **2003**, *17* (1), 87–96. https://doi.org/10.1002/RCM.858.

(78) Zenobi, R.; Knochenmuss, R. Ion Formation in MALDI Mass Spectrometry. *Mass Spectrom. Rev.* **1998**, *17* (5), 337–366.

(79) M, K.; M, G.; J, S. Ionization in Matrix-Assisted Laser Desorption/Ionization: Singly Charged Molecular Ions Are the Lucky Survivors. *J. Mass Spectrom.* **2000**, *35* (1), 1–12. https://doi.org/10.1002/(sici)1096-9888(200001)35:1<1::aid-jms904>3.0.co;2-0.

(80) Calvano, C. D.; Monopoli, A.; Cataldi, T. R. I.; Palmisano, F. MALDI Matrices for Low Molecular Weight Compounds: An Endless Story? *Anal. Bioanal. Chem. 2018 41017* **2018**, *410* (17), 4015–4038. https://doi.org/10.1007/S00216-018-1014-X.

(81) Hankin, J. A.; Barkley, R. M.; Murphy, R. C. Sublimation as a Method of Matrix Application for Mass Spectrometric Imaging. *J. Am. Soc. Mass Spectrom.* **2007**, *18* (9), 1646. https://doi.org/10.1016/J.JASMS.2007.06.010.

(82) Berry, K. A. Z.; Hankin, J. A.; Barkley, R. M.; Spraggins, J. M.; Caprioli, R. M.; Murphy, R. C. MALDI Imaging of Lipid Biochemistry in Tissues by Mass Spectrometry. *Chem. Rev.* **2011**, *111* (10), 6491. https://doi.org/10.1021/CR200280P.

(83) El-Aneed, A.; Cohen, A.; Banoub, J. Mass Spectrometry, Review of the Basics: Electrospray, MALDI, and Commonly Used Mass Analyzers. *https://doi.org/10.1080/05704920902717872* **2009**, *44* (3), 210–230. https://doi.org/10.1080/05704920902717872.

(84) AM, H. Mass Analyzers and Mass Spectrometers. *Adv. Exp. Med. Biol.* **2016**, *919*, 157–169. https://doi.org/10.1007/978-3-319-41448-5_7.

(85) Kind, T.; Liu, K. H.; Lee, D. Y.; Defelice, B.; Meissen, J. K.; Fiehn, O. LipidBlast in Silico Tandem Mass Spectrometry Database for Lipid Identification. *Nat. Methods* **2013**, *10* (8), 755–758. https://doi.org/10.1038/nmeth.2551.

(86) Caprioli, * Richard M; and Terry B. Farmer; Gile, J. Molecular Imaging of Biological Samples: Localization of Peptides and Proteins Using MALDI-TOF MS. *Anal. Chem.* **1997**, *69* (23), 4751–4760. https://doi.org/10.1021/AC970888I.

(87) Jackson, S. N.; Wang, H. Y. J.; Woods, A. S. In Situ Structural Characterization of Glycerophospholipids and Sulfatides in Brain Tissue Using MALDI-MS/MS. *J. Am. Soc. Mass Spectrom.* **2007**, *18* (1), 17–26. https://doi.org/10.1016/j.jasms.2006.08.015.

(88) Thavarajah, R.; Mudimbaimannar, V. K.; Elizabeth, J.; Rao, U. K.; Ranganathan, K. Chemical and Physical Basics of Routine Formaldehyde Fixation. *J. Oral*

Maxillofac. Pathol. **2012**, *16* (3), 400. https://doi.org/10.4103/0973-029X.102496.

(89) Carter, C. L.; McLeod, C. W.; Bunch, J. Imaging of Phospholipids in Formalin Fixed Rat Brain Sections by Matrix Assisted Laser Desorption/Ionization Mass Spectrometry. *J. Am. Soc. Mass Spectrom.* **2011**, *22* (11), 1991–1998. https://doi.org/10.1007/S13361-011-0227-4.

(90) Casadonte, R.; Caprioli, R. M. Proteomic Analysis of Formalin-Fixed Paraffin Embedded Tissue by MALDI Imaging Mass Spectrometry. *Nat. Protoc.* **2011**, *6* (11), 1695. https://doi.org/10.1038/NPROT.2011.388.

(91) Fazekas, F.; Chawluk, J. B.; Alavi, A.; Hurtig, H. I.; Zimmerman, R. A. MR Signal Abnormalities at 1.5 T in Alzheimer's Dementia and Normal Aging. *Am. J. Roentgenol.* **1987**, *149* (2), 351–356. https://doi.org/10.2214/ajr.149.2.351.

(92) Hunter, M.; Demarais, N. J.; Faull, R. L. M.; Grey, A. C.; Curtis, M. A. Subventricular Zone Lipidomic Architecture Loss in Huntington's Disease. *J. Neurochem.* **2018**, *146* (5), 613–630. https://doi.org/10.1111/jnc.14468.

(93) Sud, M.; Fahy, E.; Cotter, D.; Brown, A.; Dennis, E. A.; Glass, C. K.; Merrill, A. H.; Murphy, R. C.; Raetz, C. R. H.; Russell, D. W.; Subramaniam, S. LMSD: LIPID MAPS Structure Database. *Nucleic Acids Res.* **2007**, *35* (SUPPL. 1). https://doi.org/10.1093/nar/gkl838.

(94) Hsu, F. F.; Turk, J. Characterization of Phosphatidylinositol, Phosphatidylinositol-4-Phosphate, and Phosphatidylinositol-4,5-Bisphosphate by Electrospray Ionization Tandem Mass Spectrometry: A Mechanistic Study. *J. Am. Soc. Mass Spectrom.* **2000**, *11* (11), 986–999. https://doi.org/10.1016/S1044-

0305(00)00172-0.

(95) Han, X.; Gross, R. W. Shotgun Lipidomics: Electrospray Ionization Mass Spectrometric Analysis and Quantitation of Cellular Lipidomes Directly from Crude Extracts of Biological Samples. *Mass Spectrom. Rev.* **2005**, *24* (3), 367–412. https://doi.org/10.1002/mas.20023.

(96) McFarland, M. A.; Marshall, A. G.; Hendrickson, C. L.; Nilsson, C. L.; Fredman, P.; Månsson, J. E. Structural Characterization of the GM1 Ganglioside by Infrared Multiphoton Dissociation, Electron Capture Dissociation, and Electron Detachment Dissociation Electrospray Ionization FT-ICR MS/MS. *J. Am. Soc. Mass Spectrom.* **2005**, *16* (5), 752–762. https://doi.org/10.1016/j.jasms.2005.02.001.

(97) Caughlin, S.; Maheshwari, S.; Agca, Y.; Agca, C.; Harris, A. J.; Jurcic, K.; Yeung, K. K. C.; Cechetto, D. F.; Whitehead, S. N. Membrane-Lipid Homeostasis in a Prodromal Rat Model of Alzheimer's Disease: Characteristic Profiles in Ganglioside Distributions during Aging Detected Using MALDI Imaging Mass Spectrometry. *Biochim. Biophys. Acta - Gen. Subj.* **2018**, *1862* (6), 1327–1338. https://doi.org/10.1016/j.bbagen.2018.03.011.

(98) Stutts, W. L.; Menger, R. F.; Kiss, A.; Heeren, R. M. A.; Yost, R. A. Characterization of Phosphatidylcholine Oxidation Products by MALDI MS N. *Anal. Chem.* **2013**, *85* (23), 11410–11419. https://doi.org/10.1021/ac402400f.

(99) Wang, Z.; Cai, Y.; Wang, Y.; Zhou, X.; Zhang, Y.; Lu, H. Improved MALDI Imaging MS Analysis of Phospholipids Using Graphene Oxide as New Matrix. *Sci.*

Rep. **2017**, *7*. https://doi.org/10.1038/srep44466.

(100) Strnad, Š.; Pražienková, V.; Holubová, M.; Sýkora, D.; Cvačka, J.; Maletínská, L.; Železná, B.; Kuneš, J.; Vrkoslav, V. Mass Spectrometry Imaging of Free-Floating Brain Sections Detects Pathological Lipid Distribution in a Mouse Model of Alzheimer's-like Pathology. *Analyst* **2020**, *145* (13), 4595–4605. https://doi.org/10.1039/d0an00592d.

(101) Sipione, S.; Monyror, J.; Galleguillos, D.; Steinberg, N.; Kadam, V. Gangliosides in the Brain: Physiology, Pathophysiology and Therapeutic Applications. *Front. Neurosci.* **2020**, *14*. https://doi.org/10.3389/fnins.2020.572965.

(102) Ledeen, R. W.; Wu, G. The Multi-Tasked Life of GM1 Ganglioside, a True Factotum of Nature. *Trends in Biochemical Sciences*. 2015, pp 407–418. https://doi.org/10.1016/j.tibs.2015.04.005.

(103) Mocchetti, I. Exogenous Gangliosides, Neuronal Plasticity and Repair, and the Neurotrophins. *Cellular and Molecular Life Sciences*. 2005, pp 2283–2294. https://doi.org/10.1007/s00018-005-5188-y.

(104) Dawson, T. M.; Hung, K.; Dawson, V. L.; Steiner, J. P.; Snyder, S. H. Neuroprotective Effects of Gangliosides May Involve Inhibition of Nitric Oxide Synthase. *Ann. Neurol.* **1995**, *37* (1), 115–118. https://doi.org/10.1002/ana.410370122.

(105) Hicks, D.; Heidinger, V.; Mohand-Said, S.; Sahel, J.; Dreyfus, H. Growth Factors and Gangliosides as Neuroprotective Agents in Excitotoxicity and Ischemia. In *General Pharmacology*; 1998; Vol. 30, pp 265–273.

https://doi.org/10.1016/S0306-3623(97)00356-X.

(106) Olsen, A. S. B.; Færgeman, N. J. Sphingolipids: Membrane Microdomains in Brain Development, Function and Neurological Diseases. *Open Biology*. 2017. https://doi.org/10.1098/rsob.170069.

(107) Gouw, A. A.; Van Der Flier, W. M.; Fazekas, F.; Van Straaten, E. C. W.; Pantoni, L.; Poggesi, A.; Inzitari, D.; Erkinjuntti, T.; Wahlund, L. O.; Waldemar, G.; Schmidt, R.; Scheltens, P.; Barkhof, F. Progression of White Matter Hyperintensities and Incidence of New Lacunes over a 3-Year Period: The Leukoaraiosis and Disability Study. *Stroke* **2008**, *39* (5), 1414–1420. https://doi.org/10.1161/STROKEAHA.107.498535.

(108) Yetukuri, L.; Ekroos, K.; Vidal-Puig, A.; Orešič, M. Informatics and Computational Strategies for the Study of Lipids. *Mol. Biosyst.* **2008**, *4* (2), 121–127. https://doi.org/10.1039/b715468b.

(109) Orešič, M. Informatics and Computational Strategies for the Study of Lipids. *Biochimica et Biophysica Acta - Molecular and Cell Biology of Lipids*. 2011, pp 991–999. https://doi.org/10.1016/j.bbalip.2011.06.012.

APPENDIX

Supplementary Figures

Neuropathological Classification	***n***	***Age ± SD***	***Male Sex (%)***	***Fixation Length (months) ± SD***
Normal	5	69.4 **±** 12.9	2 (40%)	155 **±** 3.8
AD	5	75.4 **±** 5.5	3 (60%)	136 **±** 40.1
CVD	5	72.6 **±** 13.2	4 (80%)	134 **±** 39.4
AD + CVD	5	82.2 **±** 5.8	1 (20%)	160 **±** 3.1

Supplementary Table 1: Demographic data from specimen selection including neuropathological group, age at time of death, sex and fixation lengths (months since date of autopsy).

Permission

CURRICULUM VITAE

William Pinsky

Post-secondary Education:

B.M.Sc. Honours Specialization in Medical Cell Biology. 2015-2019.

The University of Western Ontario. London, Ontario, Canada.

M.Sc. Anatomy and Cell Biology. 2019-2021.

The University of Western Ontario. London, Ontario, Canada.

Honours and Awards:

CGS-M CIHR. 2020-2021.

Gold Medal for Honours Specialization in Medical Cell Biology. 2019.

Dean's Honor List. 2015-2019.

Publications:

Pinsky, W.; Harris, A.; Roseborough, A. D.; Wang, W.; Khan, A. R.; Jurcic, K.; Yeung, K. K. C.; Pasternak, S. H.; Whitehead, S. N. (2021). Regional Lipid Expression Abnormalities Identified Using MALDI IMS Correspond to MRI-Defined White Matter Hyperintensities within Post-Mortem Human Brain Tissues. *Anal. Chem.* **93**(4):2652-2659.

Dong, Y.; D'Mello, C.; **Pinsky, W.**; Lozinski, B. M.; Kaushik, D. K.; Ghorbani, S.; Moezzi, D.; Brown, D.; Melo, F. C.; Zandee, S.; Vo, T.; Prat, A.; Whitehead, S. N.; Yong, V. W. (2021). Oxidized Phosphatidylcholines Found in Multiple Sclerosis Lesions Mediate Neurodegeneration and Are Neutralized by Microglia. *Nat. Neurosci.* **24**(4), 489–503.